11-19-2008

Analysis of Pump Oil and Alkanes Evaporation

Nathaniel A. Waldstein
University of South Florida

Analysis of Pump Oil and Alkanes Evaporation

by

Nathaniel A. Waldstein

A thesis submitted in partial fulfillment
of the requirements for the degree of
Masters of Science in Mechanical Engineering
Department of Mechanical Engineering
College of Engineering
University of South Florida

Major Professor: Alex Volinsky, Ph.D.
Jose Porteiro, Ph.D.
Muhammad Rahman, Ph.D.

Date of Approval:
November 19, 2008

Keywords: Arrhenius Equation, Activation Energy, Evaporation Rates

DEDICATION

To my family, friends, and my advisor; for their encouragement made this possible.

ACKNOWLEDGEMENTS

Above all else I would like to thank my advisor Dr. Alex A. Volinsky for his support, wisdom, and unrelenting patience to whom I owe a great debt of gratitude. I would also like to thank my committee members Dr. Porteiro and Dr. Rahman for their time and advice. I am honored to have worked with Dr. Dirk C. Meyer's group at TUD and am grateful to have been privileged to use their equipment and being supplied with samples. I would also like to thank Seagate for supplying samples and give a special thanks to NSF for funding my research. Finally, I want to thank my fellow students as well as the faculty and staff in the Department of Mechanical Engineering at USF.

TABLE OF CONTENTS

LIST OF TABLES

LIST OF FIGURES

Analysis of Pump Oil and Alkanes Evaporation

Nathaniel A. Waldstein

ABSTRACT

There are many products, including hard drives, which require trace amounts, on the order of several mg, of lubricants for proper operation. The following study investigated the evaporation rates of pump oil and several alkanes, which have a wide range of applications, using a thermogravimetric machine. Both static and dynamic temperature tests were conducted. The rate of evaporation of the test specimen was determined as the percentage of mass loss per unit time. Using the Arrhenius Equation, the activation energy of the evaporation process, E_a, can be calculated as the slope of the best fit line for a plot of the ln(k) vs. 1/T (where k represents the rate of the evaporation). These values were shown to have good agreement with the enthalpy of vaporization calculated from the Clausius Clapeyron Equation and with the activation energy calculated using the Freeman and Carroll Method. The alkanes were compared using the rate of evaporation and the amount of activation energy required for evaporation as model systems. Further investigations were conducted to determine the relationship of surface area of the evaporating liquid and the rate of evaporation. It is suggested that the surface area is a function that depends on the activation, bonding, and interfacial energies of the liquid. However, the wetting angle, which aids in the description of the surface area, depends on the surface energy. Subsequent modeling was conducted in an attempt

to predict the evaporation characteristics of other lubricants for the purpose of comparison.

CHAPTER 1

INTRODUCTION TO LIQUIDS EVAPORATION

1.1 Evaporation

The conversion process from the liquid state to the gaseous state is what is known as evaporation. Liquids do not have to be heated to the boiling point in order for evaporation to occur [1-2]. The transition between the two states of matter is accomplished by molecules leaving the surface of the liquid. The molecules close to the surface of the liquid move in every possible direction at a range of varying speeds. The majority of molecules are inhibited by attractive forces within the liquid itself. Conversely, when the molecules have sufficient kinetic energy and approach the surface, at or near normal, these molecules can escape the liquid [1-2]. Although these molecules have broken through the surface of the liquid, many molecules that have evaporated reenter the liquid as a result of molecular collisions outside of the liquid. Specifically, the net vaporization is the rate at which a liquid converts to a gas. Evaporation can account for significant mass losses in an exposed liquid [3].

Since evaporation depends on kinetic energy it should be clear that as a liquid is heated, the amount of kinetic energy for individual molecules increases the evaporation rate. Regardless of temperature, a liquid that is evaporating will always be absorbing the latent heat of vaporization. In other words, an evaporating liquid will continuously absorb energy that is utilized to break molecular bonds to transform the liquid into a gas.

Molecules that successfully evaporate absorb large amounts of energy from the surrounding environment, without causing an increase in the temperature of the molecules. This results in a reduction of the temperature of the surroundings of an evaporating liquid. The rate at which the surrounding temperature reduces depends on several factors including the rate in which the molecules leave the surface of the liquid. Neglecting the contribution of other factors, an increase in the rate of molecules leaving the surface of the liquid will increase the extremity of the temperature reduction. Additionally, the molecules that remain within the liquid have lower average kinetic energies which results in a reduction of the liquid temperature. Hence, evaporation is a cooling process and it is this phenomenon that has been known and exploited for centuries. In fact, ancient Greeks and Romans used a method of hanging wet mats in windows and doorways to cool homes on hot summer days [1]. Likewise, today similar processes to this have been incorporated into many modern refrigeration systems and air conditioners.

Since evaporation requires the breaking of molecular bonds it is considered to be an endothermic process [4-5]. Any change, be it physical or chemical, that absorbs energy is termed an endothermic process [6]. How easily a liquid evaporates relates the strength of intermolecular bonds [4]. Suffice to say that the stronger the bonding the slower the evaporation rate. These bond energies represent the energetic threshold that must be met in order to break the specific chemical bond. Since bond energies represent an amount of energy absorption they are always positive [6]. Molecular structure dictates the strength of the bonds. Similar to bond energy, the amount of energy needed to be absorbed to initiate a chemical reaction, evaporation in this case, is known as the

activation energy [6]. Lower activation energies generally correlate to faster reactions and higher activation energies correlate to slower reactions.

Evaporation rates differ for different liquids and in addition to the level of activation energy required, the rate of evaporation is also determined by such things as the concentration of the surrounding gas as well as the liquid itself, the flow speed of the surrounding gas, the temperature of the liquid and the surface area of the liquid exposed to the environment. If the surrounding gas, generally air, has a high concentration of the evaporating liquid or of other substances the rate of evaporation can be significantly reduced. Likewise, if there is a high concentration of other substances, impurities, in the liquid the rate of the evaporation will also be slowed. As a liquid evaporates it gains a higher concentration of solid matter and will hence have a slower evaporation rate. Hence, evaporation can alter the intrinsic properties of a liquid; mainly the viscosity, density and amount of substances with lower molecular weights [3]. Since density is directly proportional to pressure, it too has a significant influence on evaporation rates. When the gas in contact with the surface of the liquid increases its velocity, so does the evaporation rate, and vice versa. The quality of the surrounding gas also affects the evaporation rate. For example, if the air in contact with the surface of the liquid has a high humidity then the evaporation rate will be slower than if the air was dry. An increase in the temperature of an evaporating liquid will greatly increase the rate of evaporation. Another very crucial factor in the rate of evaporation is the surface area of the liquid, that is because evaporation is a surface phenomenon; and similar to temperature, an increase in the exposed surface area greatly increases the evaporation rate.

Since temperature is arguably the most important deciding factor of the rate of evaporation, it is worth discussing further. When a liquid is at ambient pressure and at a temperature below the normal boiling point it will wet the sides of the container. In this condition the liquid will evaporate slowly and relatively steadily. If the temperature is increased to the boiling point, tiny vapor bubbles begin forming at the interface between the liquid and the container. The number of sites in which these bubbles form increases as does the rate of evaporation. That is until a certain temperature is reached above the boiling point in which the evaporation rate is at a maximum and any increase in temperature from this will actually reduce the rate. This holds true for a liquid that experiences a steady increase in temperature, but not a liquid that is vaporized by a dramatic increase in temperature [7]. The general rule when comparing different liquids is that the lower the boiling point, the more rapid the rate of evaporation.

1.2 Arrhenius Equation

The Swedish born scientist, Svante Arrhenius (1859-1927), studied at the University of Uppsala and is considered by some to be one of the founders of modern physical chemistry [8]. Arrhenius has been referred to as both a physicist and a chemist and it is in these capacities that he helped to revolutionize the science of chemistry. Some of his early writings investigated what is now called the greenhouse effect. In fact, in 1896 Arrhenius theorized the magnitude of the greenhouse effect in the *London, Edinburgh, and Dublin Philosophical Magazine*. In this publication he stated: "We are evaporating our coal mines into the air." He added that an increase of the CO_2 concentrations by as little as a factor of two, would increase the average earth's surface

temperature by about 5 °C [6]. Later in his career, in 1903, he became the first Swedish person to be awarded the Nobel Prize in chemistry for his works on the ionic theory of solution of salts [9]. Several years prior to Arrhenius winning the Nobel Prize he worked on what would later become legacy and earn him a right in the history of modern chemistry.

Arrhenius noted that the majority of chemical reactions need additional energy to continue. This energy, specifically heat energy, is added to a system until a predetermined threshold is reached and the reaction commences. This threshold is a concept that was developed by Arrhenius and is referred to as the activation energy. Arrhenius further developed these concepts and combined supportive ideas to formulate the Arrhenius equation. Simply, this equation relates the activation energy to the rate of the reaction process. Specifically, this equation was derived in order to adequately report the effects of temperature on the reaction velocities of gases [8-9]. The Arrhenius Equation was originally derived from the work of the Dutch chemist Jacobus Henricus van 't Hoff (1852 – 1911) [8]. In order for Arrhenius to explain simple chemical reactions he viewed most processes as simple 1st order reactions that have distinct temperature characteristics and obvious activation energies. These reaction fundamentals are obtained by plotting the logarithm of the rate of the reaction against the inverse of the absolute temperature. This provides a model that relates the reaction rate to temperature. One form of the Arrhenius Equation is an integration of the underlying differential equation and is presented in the following empirical expression:

$$k = Ae^{\left(\frac{E_a}{RT}\right)} \quad (1)$$

where k is a constant that correlates to the rate of the reaction, E_a is the activation energy of the reaction $\left(\frac{J}{mol}\right)$, T is the absolute temperature, R is the universal gas constant (8.314472 $\frac{J}{K\,mol}$), and A is the pre-exponential constant, which has the same units as the constant k. The units depend on the order of the reaction. For an n^{th} order reaction, the shared units are $\frac{\mathrm{mol}^{1-n}\mathrm{L}^{n-1}}{\mathrm{sec}}$. However, in this investigation the rate of evaporation was measured experimentally and has the units of mass per unit time as does the pre-exponential constant. Since the activation energy is in a nonlinear form in equation (1) problems arise during nonlinear regression. As a result, the logarithm of both sides of the equation is taken to yield:

$$\ln k = \ln A - \frac{E_a}{RT} \tag{2}$$

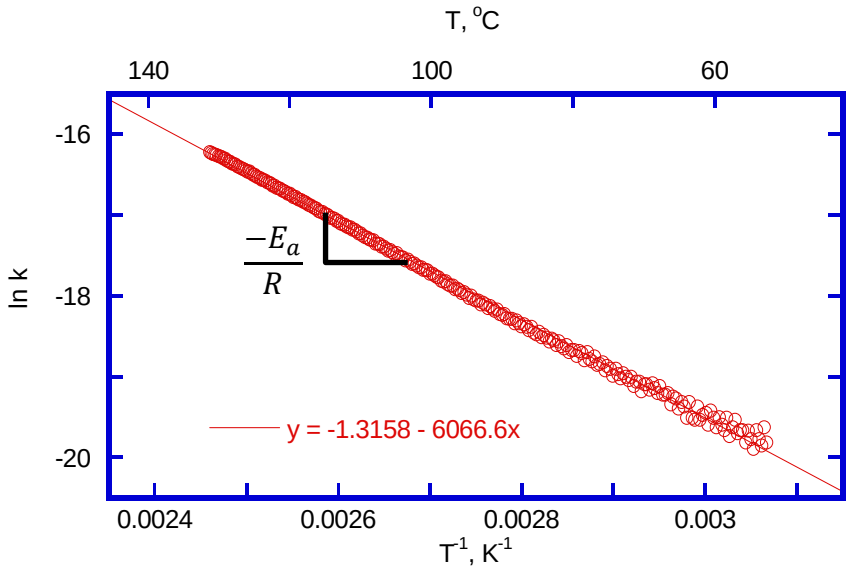

Figure 1. A typical Arrhenius Plot for the calculation of the activation energy, E_a, for the evaporation of undecane.

If the activation energy, E_a, and the pre-exponential constant, A, are unchanging with temperature then a plot of ln k against the inverse of T will result in a straight line whose slope is proportional to the activation energy and offset is logarithm of the pre-

exponential constant [10]. This can be seen if Figure 1 above. In this example, the slope of the linear best fit line multiplied by the negative of the universal gas constant provides an estimate of the activation energy of the evaporation. In this case, the activation energy of the evaporation of undecane is 50.4 $\frac{kJ}{mol}$. Likewise, taking the exponential of the offset of the best fit line provides a value of the pre-exponential constant to be 0.27 $\frac{mg}{sec}$. If the plot is not linear as previously described, then the activation energy decreases with an increase in temperature [8-9].

1.3 Clausius-Clapeyron Equation

The Clausius-Clapeyron Equation is a well-known and frequently used formula that characterizes the phase transition between two states of matter; liquid and gas in this case. Specifically it relates the heat of vaporization, or enthalpy of vaporization, to that of vapor pressure. This equation is named after the prominent German physicist and mathematician Rudolf Julius Emanuel Clausius (1822 – 1888) and the French engineer and physicist Benoît Paul Émile Clapeyron (1799 – 1864) [11-12]. Both men are considered to be founders of the science of modern thermodynamics with their individual and contributing works on what is now known as the second law of thermodynamics.

Two very important terms should be defined prior to continuing a discussion on the Clausius-Clapeyron Equation. The first of which has been used previously in this section, and that is the heat of vaporization. According to [13], the heat of vaporization is "the amount of heat required to vaporize one gram of a liquid at its boiling point with no change in temperature". More generally, enthalpy is the amount of potential heat in a substance and it is proportional to pressure and volume. Therefore, the heat of vaporization (ΔH) can be thought of as the energy requirement for the transformation of a

given amount of substance, from the liquid to the gaseous state. This value is conventionally measured at the normal boiling point of the substance. However, most tabulated values are adjusted to a temperature of 298 K.

Vapor pressure is "the particle pressure of a vapor at the surface of its parent liquid" [13]. To explain further, when a vapor is in thermodynamic equilibrium with non-vapor phases then the pressure of this vapor is referred to as vapor pressure. Under certain circumstances, all liquids and even some solids have the propensity to evaporate and transform into the gaseous state. Likewise, all gases, under similar circumstances, tend to condense to the original state, be it liquid or solid. For a specific substance at a specific temperature there will exist a pressure at which the evaporated gas is thermodynamically in equilibrium with the condensed form (liquid or solid). This is known as the vapor pressure for the specific substance at that particular temperature. Volatile substances are those that have a high vapor pressure at near atmospheric pressures. The vapor pressure indicates the required pressure in order to have equilibrium, which relates the readiness of molecules to escape from the surface of the liquid. Therefore, this equilibrium pressure or vapor pressure is an indicator of the evaporation rate of a liquid.

Understanding these terms it is now necessary to establish a relationship between the heat of vaporization and what is referred to as the pVT behavior of a fluid [14]. The most basic relationship approximating the pVT behavior of real fluids was established by the Dutch physicist and Nobel laureate Johannes Diderik van der Waals (1837 – 1923) [15]. The van der Waals equation can be represented in the following form:

$$p = \frac{RT}{V-b} - \frac{a}{V^2} \tag{3}$$

where both a and b are characteristics of the specific substance. Instead of now iteratively relating the pVT behavior to that of the heat of vaporization, a more often used method that provides a relationship between the heat of vaporization (ΔH) to that of the temperature dependence of the vapor pressure (p) will follow.

First it should be noted that equation (3) is considered to be valid in a single-component system (one substance) at equilibrium between vapor and liquid. Analyzing the Gibbs energies in this situation reveals that the differential Gibbs energies of the saturated liquid and the saturated vapor are equal. Symbolically:

$$dG^l = dG^g \tag{4}$$

The total differential Gibbs energy is provided by the following relationship:

$$dG = -SdT + Vdp \tag{5}$$

where S is the molar entropy, V is the molar volume, T is the temperature, and p is the vapor pressure. Combining these two equations provides a relationship between the heat of vaporization and the derivative of the vapor pressure with respect to the temperature along the saturation curve. This relationship is better known as the Clapeyron Equation and the empirical form and its derivation is as follows:

$$-S^l dT + V^l dp = -S^g dT + V^g dp$$

$$(S^g - S^l)dT = (V^g - V^l)dp$$

$$\left(\frac{dp}{dT}\right)_{sat} = \frac{S^g - S^l}{V^g - V^l}$$

$$\left(\frac{dp}{dT}\right)_{sat} = \frac{H^g - H^l}{T(V^g - V^l)}$$

$$\left(\frac{\Delta S}{\Delta V}\right)_{sat} = \frac{\Delta H}{T\Delta V} = \left(\frac{dp}{dT}\right)_{sat} \quad (6)$$

From this equation it can be determined that when both the heat of vaporization and the change in volume are positive, the vapor pressure will always increase with increasing temperature [14]. Integration of the Clapeyron Equation provides an exact relationship that relates the dependence of the vapor pressure on the temperature, in a certain range. This range is the region from the triple point temperature to that of the critical temperature. This region can be viewed on a phase diagram of the substance. To explain, a phase diagram is a plot of pressure against temperature that illustrates the conditions for which a given phase of the substance exists [16]. Figure 2 shows an example of a phase diagram for water. On this plot there are two important points: the triple point (A) and the critical point (C). The triple point determines the necessary temperature and pressure needed for all three phases to coexist. The critical point, on the other hand, specifies at what temperature and pressure the substance must be in order for a phase boundary to no longer exist. Considering a closed system composed of liquid and vapor that is heated; as the temperature increases the density of the liquid reduces and the density of the vapor increases. The temperature at which the two densities are equal is the critical point. The heat of vaporization is zero at and beyond the critical point and the liquid state cannot exist passed it [16].

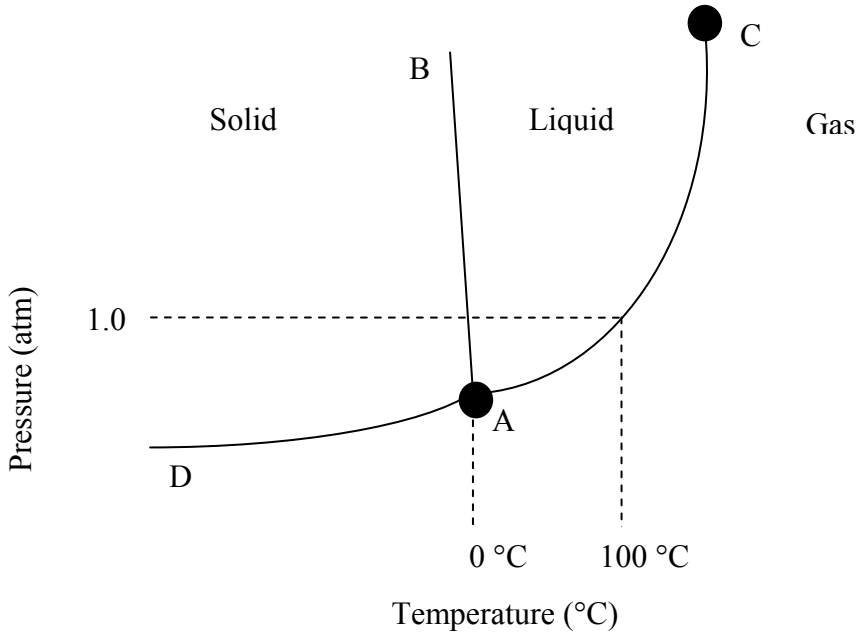

Figure 2. Water phase diagram.

Returning to the specifics of the Clapeyron Equation; a reduction in the pressure the culminating effects of the pVT behavior of the liquid phase becomes increasingly insignificant. Understanding this is the basis of the Clausius-Clapeyron Equation. The Clausius-Clapeyron Equation is a rather restrictive yet useful method of relating the heat of vaporization to that of vapor pressure and takes the following form:

$$\ln p = -\frac{\Delta H_{vap}}{RT} + C \qquad (7)$$

where C is a constant of integration. A key simplification inherent to this equation is that the volume of the vapor is formulated by the ideal gas equation of state and this volume is significant enough, as compared to the volume of the liquid, that the latter has been neglected. As previously stated, this equation is often used to estimate the relationship between the heat of vaporization and the vapor pressure, and a quick survey of equation (7) should relate the ease of these estimations and convey its convention. A result that is

inherent to this equation is that for temperatures below the normal boiling point, the calculated heat of vaporization will always be higher than the correct values, with an associated error of less than 5% [14].

Taking a differential form of the Clausius-Clapeyron Equation:

$$\frac{d\,\ln p}{d\left(\frac{1}{T}\right)} = -\frac{\Delta H_{vap}}{R} \tag{8}$$

and integrating this with the assumption that the heat of vaporization is a constant provides:

$$\ln p = A + \frac{B}{T} \tag{9}$$

where A is a constant of integration and the variable B is constant. Since the logarithm of the vapor pressure is only linear in small range of temperatures, equation (9) will not exactly describe the behavior of a substance [17]. There are numerous semi-empirical equations that modify the right-hand side of equation (9); a review of which can be found in [18]. However, the form of this equation, originally published by Antoine [19], that was used in this research takes the following form:

$$\ln p = A + \frac{B}{T} + C\ln T + DT + ET^2 \tag{10}$$

where p is the vapor pressure (mm Hg), T is the temperature (K), and the variables A, B, C, D, and E are all constants specific to substances and are valid within a determined temperature range. This form of the Antoine Equation is more expanded than the general form, but both provide accurate representations of substances over a large range of temperatures as shown in [20].

The constants of the Antoine Equation, or Antoine Constants, are known and tabulated for many substances and tabulated values were used in this research for the six

n-alkanes. However, the pump oil that was investigated is was of an unknown composition. Therefore the constants are not tabulated and this approach was not used with the pump oil . The Antoine constants of the n-alkanes were obtained from [21] and can be found in Table 1; along with the valid temperature ranges, and names of each n-alkane studied.

Table 1. Antoine Constants and valid temperature range for alkanes.

Alkanes	A	B	C	D	E	Range (K)
Undecane	82.923	-5608.5	-27.327	1.05E-02	7.09E-13	247.6 - 638.8
Dodecane	-5.6532	-3469.8	9.0272	-2.32E-02	1.12E-05	263.6 - 658.2
Tridecane	49.239	-4964.9	-13.769	-2.11E-09	2.59E-06	267.8 - 675.8
Tetradecane	106.11	-7346.1	-35.195	1.24E-02	-8.40E-13	279.0 - 692.4
Pentadecane	116.52	-8041	-38.799	1.34E-02	-4.44E-13	283.1 - 706.8
Hexadecane	99.109	-7533.3	-32.251	1.05E-02	1.23E-12	291.3 - 720.6

From Table 1 it can be seen that the maximum low temperature that is considered valid for all the alkanes is 291.3 K or about 18.2 °C. Similarly, the minimum high temperature that is valid for all the alkanes is 638.8 K or about 365.7 °C. This means that as long as testing is done between 18 and 366 °C, the approximations of the vapor pressure for all of the alkanes are valid and reasonably accurate. Since the vapor pressures are first estimated then used in the Clausius-Clapeyron Equation to calculate the heat of vaporization, this implies that the values of heat of vaporization are also valid and accurate within this temperature range.

Another method for estimating the heat of vaporization is to use Trouton's Rule [22-23]. Trouton's Rule is a rough approximation and is mainly used as a quick reference to ensure results are close to expected values. Suppose there is a liquid vapor system in

equilibrium and the vapor pressure is allowed to reach 1 atm. At this point the liquid will boil and completely transform into a vapor once it has absorbed the heat of vaporization and the temperature at which this occurs is its normal boiling temperature. The approximate relationship between the normal boiling point and the heat of vaporization is known as Trouton's Rule and is as follows:

$$\frac{\Delta H}{\mathrm{T}_b} = 21 \ \frac{cal}{mol\ K} \tag{11}$$

or,

$$\frac{\Delta H}{\mathrm{T}_b} = 87.9 \ \frac{J}{mol\ K} \tag{12}$$

where T_b is the normal boiling point of the substance. Since all the alkanes have well documented characteristics it is possible to gain rough estimates of the heat of vaporization of each individual alkane based on the tabulated values of the normal boiling temperatures. Table 3 lists each alkane and their corresponding boiling temperature obtained from [21] and the heat of vaporization estimated by use of Trouton's Rule.

Table 2. Heat of vaporization of alkanes from Trouton's Rule.

Alkanes	T_b (°C) [21]	$\Delta H \left(\frac{kJ}{mol}\right)$
Undecane	195.5	41.2
Dodecane	216.0	43.0
Tridecane	234.0	44.6
Tetradecane	253.5	46.3
Pentadecane	270.5	47.8
Hexadecane	287.0	49.2

1.4 Alkanes

Alkanes are organic compounds that only contain carbon and hydrogen atoms. They can sometimes be referred to as aliphatic compounds or paraffins. Alkanes are considered to be a non-functional group due to a relative unreactive nature and do not experience many chemical reactions. All bonds between both carbon atoms (C-C) and carbon and hydrogen atoms (C-H) in alkanes are referred to as single, sigma (σ) bonds [23]. Sigma bonds are formed from the overlapping of atomic orbitals. The total overlap of the bonding orbitals is proportional to the strength of a bond. The two main sources of alkanes are crude oil and coal. The primary uses of alkanes are for fuels. The majority of alkanes are known as acyclic and acyclic materials are classically divided into two separate subcategories: straight chains and branched chains. Straight chains are aptly named because they are a straight series of carbon atoms connected to one another. Branched chains, on the other hand, have other connective groups of chains of carbon atoms that extend off of the original chain. These connective groups are commonly

referred to as side chains or simply branches. Figure 3 illustrates both straight chain and branched chain alkanes. All of the alkanes that were tested are straight chain molecules.

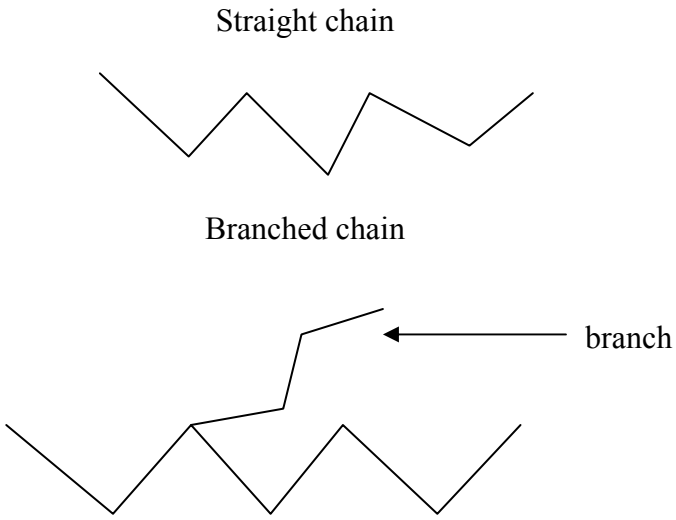

Figure 3. Differences between straight chain and branched chain alkanes.

In addition to acyclic, alkanes can be cyclic in that the carbon atoms form rings. These specific alkanes are termed cycloalkanes and since they are of a different type of alkane as the research samples they will not be further discussed, but a review of these types of alkanes can be found in [24].

The formulas and structures of alkanes are another example of distinctive characteristics. In a given compound alkanes contain the maximum number of hydrogen atoms in connection with carbon atoms. It is for this reason that alkanes are deemed saturated compounds, because they are *saturated* with hydrogen atoms. Table 2 shows the list of alkanes of this investigation and the associated molecular formula. The formulas increase one CH_2 unit for every successive alkane. Table 2 is known as a homologous series and each separate molecule is known as a homolog. The general formulation for alkanes is C_nH_{2n+2} [24].

Table 3. Molecular formulas of alkanes.

Alkanes	Molecular formula	Condensed formula	Molecular Weight $\left(\frac{g}{mol}\right)$
Undecane	$C_{11}H_{24}$	$CH_3(CH_2)_9CH_3$	156
Dodecane	$C_{12}H_{26}$	$CH_3(CH_2)_{10}CH_3$	170
Tridecane	$C_{13}H_{28}$	$CH_3(CH_2)_{11}CH_3$	184
Tetradecane	$C_{14}H_{30}$	$CH_3(CH_2)_{12}CH_3$	198
Pentadecane	$C_{15}H_{32}$	$CH_3(CH_2)_{13}CH_3$	212
Hexadecane	$C_{16}H_{34}$	$CH_3(CH_2)_{14}CH_3$	226

There are also many physical and chemical properties that set alkanes apart from other compounds. As mentioned, alkanes consist of only C-C and C-H bonds of which the C-C bonds are nonpolar and the C-H are essentially nonpolar. This means that the molecules are nonpolar and as such are soluble in nonpolar solvents, like other alkanes, and are immiscible in polar solvents, like water. The C-H bond is a fairly strong bond and since it is considered nonpolar it makes the alkane molecules less reactive than polar molecules. Alkanes are less dense than water at room temperature and as a result are characterized as hydrophobic compounds. Alkanes are generally chemically inert, which allows for stability over long periods of time. Alkanes also have the propensity to react with oxygen or burn when presented with a source of ignition; hence, alkanes are used as fuels.

Another characteristic of alkanes resulting from the nonpolarity of the molecules is that the intermolecular attractions are created by London dispersion (LD) forces [24]. When compared to polar intermolecular attraction forces, hydrogen bonding and ionic bonding, LD forces are considerably weaker. Fluctuations in electron densities generate transient dipoles, which are responsible for the LD forces. As the molecule increases in

size so does the significance of the effect of the LD forces. Generally, the lower the molecular weight of the alkanes, the smaller the total intermolecular forces are, and if the total forces are small enough, the alkanes will be a gas at room temperature. However, larger molecules inherently have a larger total of intermolecular forces which are necessary for alkanes to be liquids at room temperature. Higher molecular weights result in even greater total intermolecular forces and the resulting alkanes will be solids at room temperature. As the molecular weight increases, the intermolecular forces increase resulting in a higher boiling point and melting point. Conversely, branched molecules often boil and melt at significantly lower temperatures due to decreased intermolecular forces. This also means that less energy is required by branched molecules to complete a phase transition.

CHAPTER 2

EVAPORATION TEST METHODS

2.1 Testing methods

There are a number of ways to measure the evaporation rates of substances. When measuring characteristics of a substance, or substances, the testing variable that is deemed most important is what dictates the method of measurement. In the case of the evaporation rate of liquids there are three main variables of importance which are: the temperature of the substance, the amount of substance, and the vapor pressure of the evaporated liquid. The following is a quick review of some of the more popular methods of determining evaporation rates from these three approaches.

If the testing variable of temperature is determined to be the most important then a method that conforms to the thermodynamic principle of evaporative cooling follows. In this approach a cloth or gauze pad is dipped into a container of the testing sample. The pad is usually wrapped around a thermocouple prior to the submersion because the liquid will begin evaporating as soon as it is removed from the container. As soon as the thermocouple and soaked gauze pad are removed from the container the liquid begins evaporating and as discussed in section 1.1 it will also begin cooling. Monitoring the cooling rate of the substance, exposed to normal ambient conditions, provides a temperature profile of the evaporation process of the substance. This information can then be used to determine the specific latent heat of the substance. Latent heat is the

amount of energy absorbed during a phase transition, evaporation in this case. Knowing such tabulated variables as the density of the vapor, the thermal conductivity of the liquid and the vapor, and together with an understanding of the temperature profile will give the specific latent heat of the substance directly. The amount of energy absorbed during a phase change is equal to the specific latent heat of the substance multiplied by the mass of the sample. Since bond energies can be thought of as the amount of energy required to break the intermolecular attractions of a substance than this is a good indication of the heat of vaporization and can be representative of the evaporation rate. This procedure is very cost effective because the only required equipment is a thermocouple and a computer. For repeatable results, the testing must be done in the same ambient conditions for every test. For example, the temperature, quality, and velocity of the air in the lab must be maintained constant during testing. For more information on this type of evaporation testing please see [4-5].

Another approach focuses on the quantity of the sample, or more precisely, the amount of loss of the sample with respect to time. This methodology follows the principles of thermogravimetrics to estimate the evaporation rate of the sample. This can be achieved by a number of techniques and by several different testing apparatuses. In general, this approach measures the mass loss of the sample continuously with time and temperature. The mass is measured with a highly sensitive device that can detect minor changes, on the order of 0.1 μg sensitivity [32]. When the substance is a liquid the mass loss represents the amount of the sample that is being evaporated and when the substance is a solid the mass loss represents the amount of the sample that is sublimated. As a result of monitoring the time lapse in addition to mass loss, the recorded mass loss is easily

transformed into a rate of phase transformation (evaporation or sublimation). Depending on the particular setup, this type of testing can be done in a vacuum or in a sealed chamber with or without a purging gas. Regardless of setup, as before, conditions must remain constant between testing runs to ensure repeatability and ultimately comparability between samples. This approach requires expensive instrumentation and licensed data analyzing software. For further information on this specific testing approach see [10, 25, 32].

Yet another way to determine a compounds specific evaporation rate is to directly measure the vapor pressure of the evaporated liquid. This approach assumes that a liquid vapor system in equilibrium will provide necessary information of the evaporation process. In this method the sample must be in a closed liquid vapor or solid vapor system. The closed system is then evacuated of the trapped air creating a vacuum. As the sample evaporates in the vacuum chamber, the vapor pressure can be measured directly by a couple of different means; which depend on the particular testing arrangement. In [26] a wire fed into the vapor portion of the vacuum chamber will change its resistance as the vapor pressure changes. This changing resistance can be calibrated by known substances to give accurate readings of the changing vapor pressure. Once an accurate vapor pressure profile is obtained, the use of the Clausius-Clapeyron equation will provide valid approximations of the evaporation rate of the samples. This procedure is less costly than the thermogravimetric approach, but requires the ability to create a vacuum. However, since the testing is done in and the readings are taken from a vacuum, then it is very easy to maintain constant environmental conditions between testing and is the most readily

comparable approach; in terms of direct measurements. A good review of this approach can be found in [26-27].

2.2 Testing procedure

All testing followed the same procedure and used the same testing equipment. Samples were taken from storage containers using a p200 micropipette, 9 mg for alkane testing and 20-25 mg samples were drawn for pump oil tests. The micropipette was then used to inject the samples into aluminum pans and the pans were then placed onto a microbalance. The pan with the sample was balanced with an empty identical aluminum pan and the microbalance was zeroed. The particular microbalance used in this experimentation has a resolution of 0.001 mg, a range of ± 500 mg, and a maximum gross sample weight limit of 1 g. The pans were then heated inside a heating chamber with a programmable temperature profile and the differential temperatures were recorded. Thermocouples were utilized to measure the temperature of the empty pan and the pan that contained the sample substance, as well as the temperature inside the heating chamber. The chamber is isolated from the atmosphere and the inside temperature is used as a baseline temperature. The difference in temperature of the two pans was then used to accurately determine the temperature of the sample to within 1 °C. The temperatures and the weight of the sample were measured continuously throughout testing runs. The testing runs were concluded when the sample was completely evaporated or until the heating program ended. The equipment used during testing was highly accurate and proved to be a very good comparative tool for the evaporation of different substances.

CHAPTER 3

ALKANES AND OIL EVAPORATION RESULTS

3.1 Evaporation measurements

Evaporation measurements, regardless of the testing approach, depend on several very important factors. These factors must be held as constant as possible to ensure repeatability between testing and comparability between results. Without proven repeatable testing the results are invalid and a good understanding of the process of interest is not obtained. As a result, without proven repeatability results of different testing runs and between different samples cannot be compared.

3.1.1 Repeatability studies

The most important factors of evaporation measurements have been determined by most of the literature, specifically [25, 28-31], and our own testing. These factors are the initial mass of the samples, the exposed surface area of the samples, the heating rate of the testing procedure, the flow rate of the surrounding gases (if applicable), the vapor pressure produced by the evaporative process, the molecular weight of the substances being tested, and the temperature (both the range and the specific temperatures during testing). The majority of these factors can be readily maintained as constants between testing cycles with the exception of the vapor pressures and molecular weight which depend on the particular substance being tested.

The heating rate and temperature are the easiest of the factors to keep constant between testing. For a lot of testing apparatuses a testing run must first be established prior to testing. This acts as the blueprint of testing that the instrument will follow until stopped or the procedure has run its course. The instrument must have certain inputs from the user such as to what temperature should the sample be heated or cooled to, at what rate should this be done, should the sample be held isothermal after reaching this temperature, and if so, for how long, etc. Once the user has determined these inputs a testing procedure has been established and is entered into the computer. If this procedure provides satisfying results then it can become the procedural guidelines for all the testing and thus the heating rates and temperatures will be the same for the testing of all samples.

Figure 4 illustrates a sample portion of the testing procedure utilized for the many tests of the pump oil in different arrangements. The testing was done for over 70 hours while varying the temperatures but keeping the heating and cooling rates constant at 20 °C/min and – 30 °C/min, respectively. The pump oil was either experiencing standard pan evaporation or was evaporated from micro-fluidic channels. As Figure 4 shows, the temperature was held isothermal after each temperature increase or decrease for a period of 1 hour. This allowed enough time for the temperature to stabilize before increasing or decreasing. This is crucial for sampling static temperatures rather than dynamic or rapid fluctuations of temperature. Conversely, Figure 5 demonstrates what has been deemed as static testing. Figure 4 shows a rather rapid increase in temperature to effectively evaporate the sample completely in a short amount of time. The time duration of this type of testing was generally around 10 minutes. It should be noted that both Figure 4 and Figure 5 are plots of the sample temperature with time, not the instrumentation

temperature. As a result there are distinct nonlinearities in these two graphs. In Figure 4, just after a temperature increase or decrease, obvious temperature oscillations can be seen. This is due to a fluctuating sample temperature prior to stabilization at the set isothermal temperature. Figure 5, however, has two regions of the graph that are nonlinear. The first region is occurs in the first minute of testing and this nonlinearity is due to the thermal inertia of the sample. In other words, there is a time delay between heating the sample and the sample temperature increasing. The second region of nonlinearity occurs at about 6 minutes, for this example, and this correlates to when the sample mass is 10 - 20% of the initial mass, depending on the alkane. Once the sample has been evaporated completely, the temperature increase of the instrumentation increases more proportionally with the empty pan resulting in a nonlinearity and a subsequent change in slope.

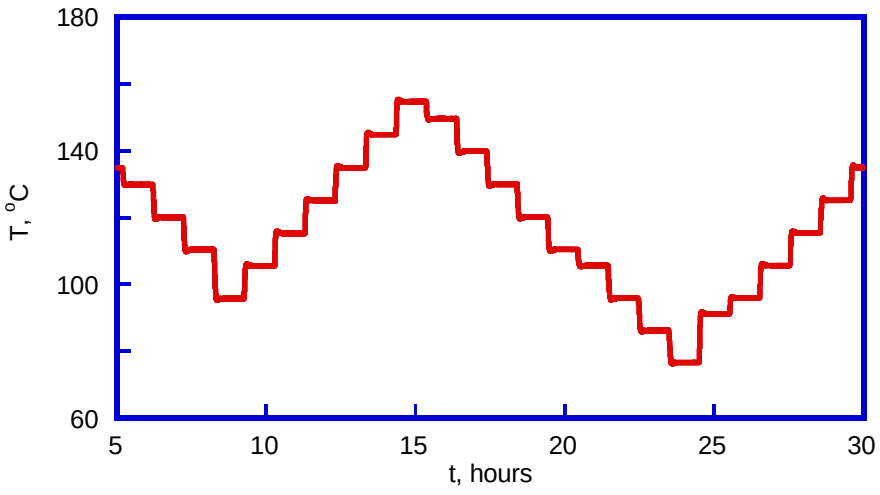

Figure 4. Example of the pump oil testing procedure, temperature profile.

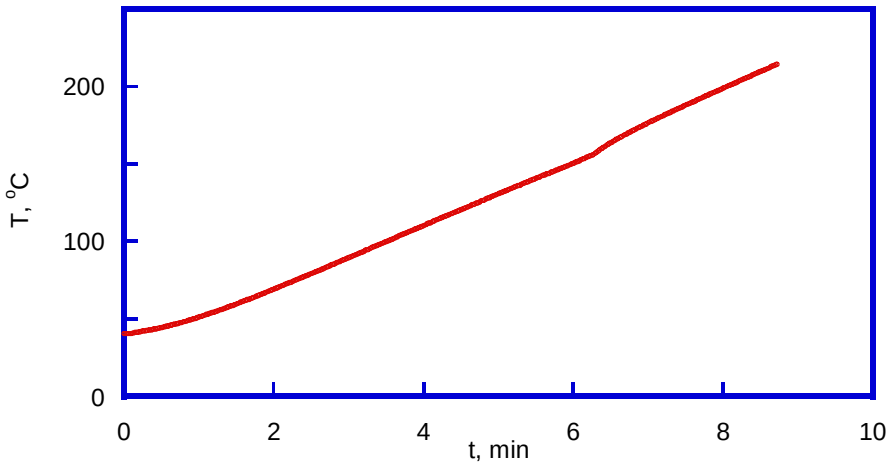

Figure 5. Example of the dynamic alkane testing procedure, temperature profile

The heating rate also has a profound effect on the accuracy of the calculated activation energies. In general, when a sample is heated using a particular procedure, if the heating rate is too slow then the values of the activation energies are not as repeatable [25, 28-31]. From this it can be expected that different heating rates will result in different values of activation energy. However, when the heating rate is above 10 °C/min, for example, the activation energies will have less deviation. Table 4 displays just that for some of the alkanes tested. As Table 4 shows, the heating rates used for different testing notice how as the rate increases the conformity of the activation energy calculations becomes more acute.

Table 4. Alkanes activation energy, E_a, calculated for different heating rates from the Arrhenius Plot.

Heating rate (°C/min)	Undecane E_a $\left(\frac{kJ}{mol}\right)$	Dodecane E_a $\left(\frac{kJ}{mol}\right)$	Tridecane E_a $\left(\frac{kJ}{mol}\right)$
0.5	51.7	50.1	50.7
1.0	58.2	57.9	59.4
3.0	55.2	56.6	56.3
5.0	56.7	54.4	55.2
10.0	52.7	54.0	54.5
20.0	53.0	56.1	54.9
30.0	51.8	54.4	55.1

As discussed in section 1.1, the heating rate also affects the rate of evaporation. It should be obvious that the higher the rate of temperature increase the faster the sample will evaporate. A series of testing was completed to better understand the dependence of the rate of evaporation to that of the heating rate. The initial mass was kept relatively the same for each test ± 0.5 mg. However, to ensure conformity between testing the percentage of mass loss is preferred. Each test was conducted in a burn-like procedure in which the temperature was ramped to the same value of 200 °C, but with varying heating rates. The result for undecane can be seen in Figure 5. As expected, faster heating rates result in less time for the sample to completely evaporate.

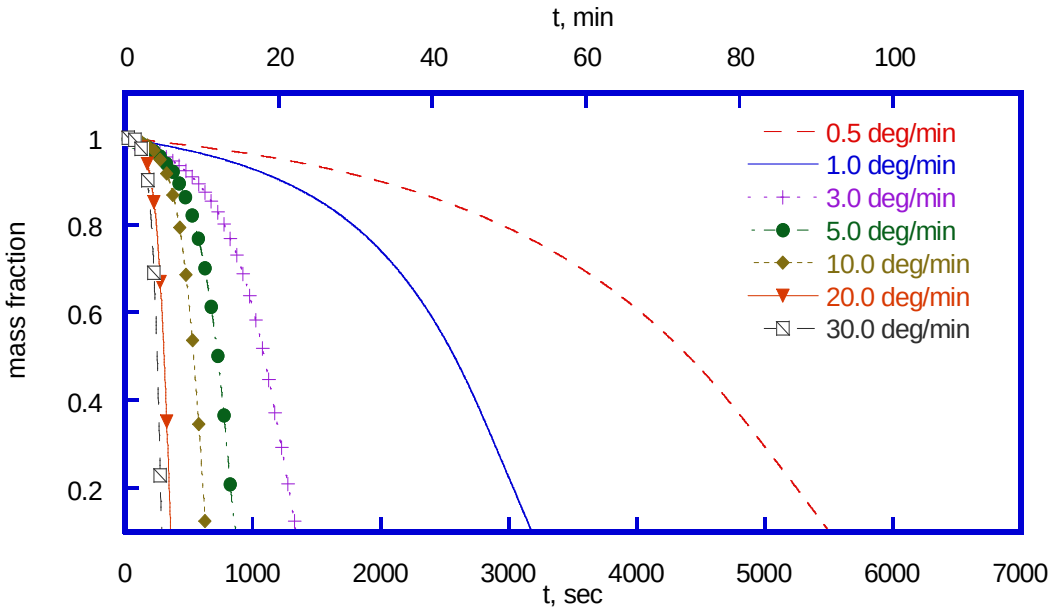

Figure 6. Heating rate dependence for undecane.

The flow rate of the surrounding air also has a dramatic impact on the overall evaporation process. For example, Figure 7 shows the difference between the same test with and without a cooling fan on. The testing sample was the pump oil and the air flow rate of the fan was approximately 25 mL/min, and the temperature testing procedure was the same for both tests. Figure 7 illustrates a distinct difference in the use of a fan to increase the speed of the surrounding air. As previously mentioned in section 1.1, the flow rate of the air in contact with the exposed liquid greatly affects the rate of evaporation. Using the linear best fitting lines from Figure 6, it can be determined that the activation energy without air flow is about 83.6 $\frac{kJ}{mol}$ and with air flow is approximately 59.6 $\frac{kJ}{mol}$. This equates to a 24 $\frac{kJ}{mol}$ reduction in the amount of energy needed to break the intermolecular attractions in order for the liquid to evaporate. The pre-exponential constant is reduced by an even greater amount. With the 25 mL/min air flow the pre-

exponential constant is approximately 6.9 $\frac{mg}{sec}$ and without the air flow the pre-exponential constant is closer to 1.4e-4 $\frac{mg}{sec}$. This demonstrates just how significant the flow rate of the surrounding air is to the characteristics of evaporation.

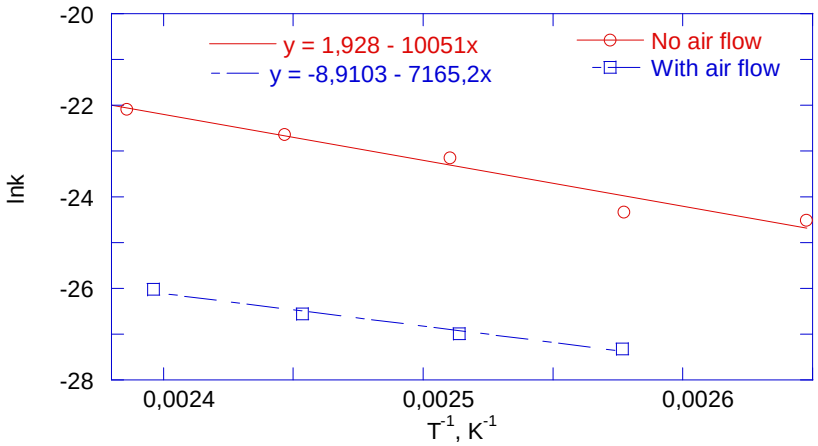

Figure 7. Comparison of oil evaporation rate with and without air flow.

As previously mentioned, the initial mass of the sample is a very important factor when attempting to obtain repeatable testing results. To ensure repeatable initial masses a micropipette was used. After several testing iterations the lack of accuracy of the micropipette was made evident. It was necessary to reset the micropipette each time prior to use. However, setting the micropipette to the same value every time did not result in the same amount of liquid being retained. It was initial thought that the micropipette was taking the same volume of liquid each time, but due to density changes between samples the amount of mass changed. This may in fact be true, but upon further inspection, using the same alkane resulted in different initial mass measurements. To better explain, a series of constant mass testing was conducted in which each alkane was tested numerous times using the same micropipette value prior to obtaining the sample. This was repeated

for every alkane. The results for undecane, for example, were a maximum value of 9.4 mg a minimum value of 8.1 mg with an average value of 9.0 mg and a standard deviation of 0.5 mg. These variations in initial mass, however small, would ultimately result in erroneous calculations of the activation energies of the alkanes. To combat this problem the data were analyzed by using the amount of mass reduction as a percentage of the initial mass per unit time. Simply dividing the instantaneous mass measurement by the initial mass reading provides the percentage of the initial mass remaining at a specific time. This was done for all the testing of the alkanes and the pump oil. Figure 8 shows a graphical representation of this correction result. In this figure there is a plot of the mass loss as a percentage of the initial mass versus time for every alkane. The alkanes were ramped to the same high temperature at a rate of 20 °C/min and this testing procedure was constant for each testing cycle. Figure 8 provides a good estimation of comparison of the different alkanes' evaporation rates.

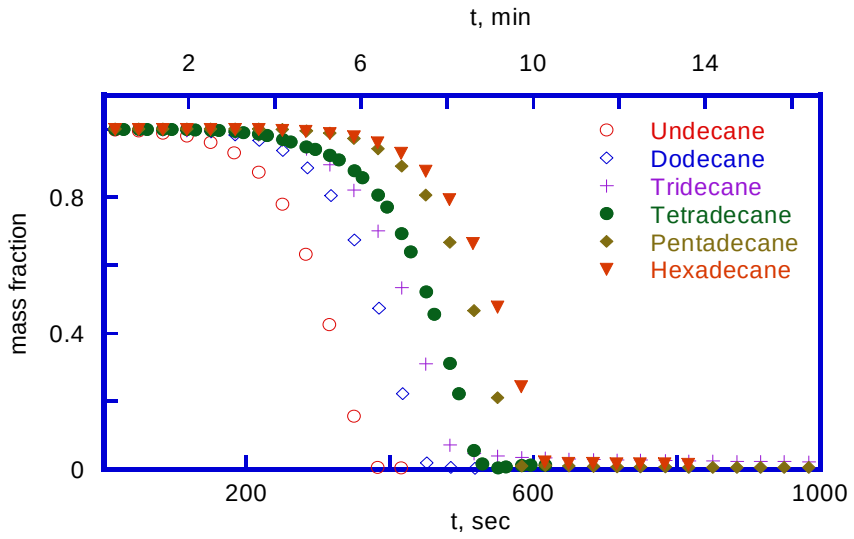

Figure 8. Mass loss as a percentage of initial mass for each alkane.

Finally, the surface area of the exposed liquid is a very important factor that must be controlled to promote repeatability and to compare final results. The exposed surface area was relatively the same for each alkane and the pump oil because all testing was done in aluminum pans of the exact same dimensions. Through repeated use the pans did become slightly deformed changing the overall shape of the opening of the pan. This change in dimension was determined to have very little effect on the exposed surface area. In order to estimate the surface area of the liquid in the pan, the pan dimensions, the wetting angle, and the height difference between the liquid at the inner sides of the pan, and the center of the pan must all be known. The pan dimensions are easily obtained from the manufacturer's data or can be physically measured. The pans that were used had an inner diameter of 5 mm and an inner height of 1.5 mm. The wetting angle came from a profile measurement using an optical microscope. The profiles were measured by focusing the image of the sample surface in the microscope and noting the position of the lens. The sample was then incrementally moved and as the changes in the focal lengths were recorded an estimate of the profile of the liquids were obtained. The scanning of the liquid surface was conducted from the liquid pan interface of one side of the pan to the other. From this profile the height difference between the liquid at the sides of the pan and the center of the pan could easily be calculated. It is important to take note of another simplifying assumption that was used in the calculation of the exposed surface area. This simplification is that due to close molecular composition and densities of the alkanes it has been assumed that the deviation in wetting properties between them is negligible. So to gain an average representation of the wetting profiles of the alkanes, tridecane was used to calculate the wetting angle and exposed surface area. Tridecane was used because

the average density of the alkanes is 0.758 $\frac{mg}{\mu L}$ and the average molecular weight is 191 $\frac{g}{mol}$, whereas tridecane has a density of 0.756 $\frac{mg}{\mu l}$ and a molecular weight of 184 $\frac{g}{mol}$. Figure 9 is a picture of the pump oil in the test pans. From left to right in Figure 9 is an example of fresh oil, oxidized oil, and burnt oil. Fresh oil is oil that was taken directly from its container and injected into the pan, oxidized oil is oil that has been run through a series of heat treatments but has not completely evaporate and burnt oil is oil that experienced a rapid increase in temperature and what is left inside the pan are carbon deposits.

Figure 9. Example of wetting profile of three stages of oil.

Figure 10 shows the recorded profile from the optical microscope of tridecane with the center point of the pan being at 2.5 mm and 0 mm and 5 mm representing the inner surfaces of the pan walls. The recorded data points for the profile have been fitted with a fourth order polynomial and the equation can be found in Figure 10. From Figure 10 it can be determined that the minimum height of tridecane is 0.60 mm and a maximum of 1.12 mm. Figure 11 illustrates a similar result for the pump oil. The profile of the pump oil yields a maximum height of 1.41 mm and a minimum height of 0.53 mm.

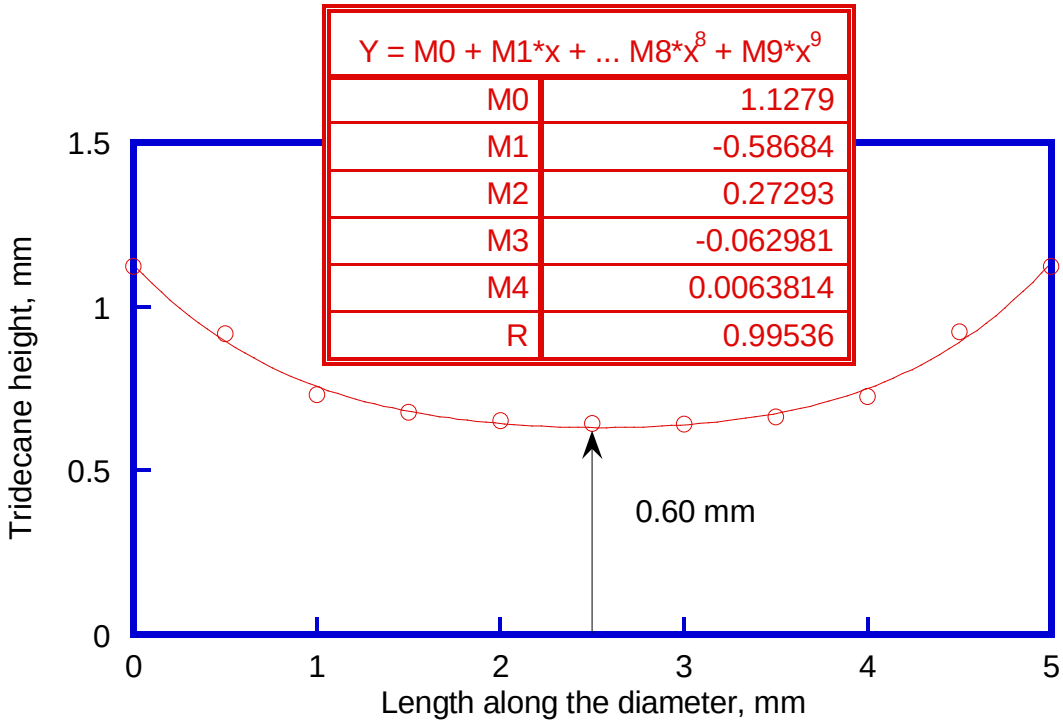

Figure 10. Wetting profile of tridecane in a pan.

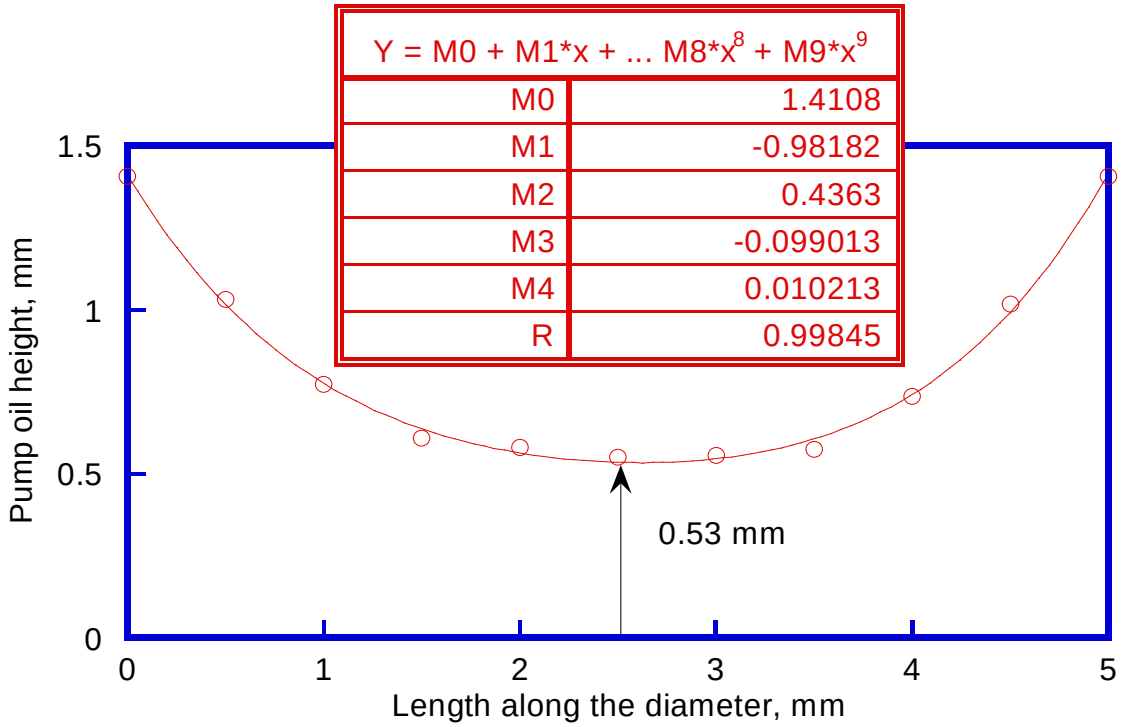

Figure 11. Wetting profile of pump oil in a pan.

The wetting angles for these two substances were estimated from an averaging of angles. In this method the lowest point of the liquid profile is selected as a reference point. The angle between this point and the next is determined by simple trigonometric identities. The angle of between the second point and the third point is then found. This is repeated until the angle between the last two points is recorded. The summation of these angles is recorded and the average is calculated. This process is repeated for both sides of the minimum point and for both liquids. The average of each side was then averaged with the other to give an overall average estimate of the wetting angle for the two liquids. Using this approach, the wetting angles for tridecane and the pump oil are 10.55° and 17.71°, respectively. As expected the sample with the higher molecular weight, density, and viscosity has the higher wetting angle. To better express the difference in the measured wetting angles of tridecane and pump oil Figure 12 was constructed. Figure 12 is displays the profile of tridecane and pump oil superimposed onto the same plot. Notice the similarity of the overall shape of the two profiles, but they differ in angle and minimum height of the liquid. These nonconformities are due to the differences between the surface energies and densities of the two liquids.

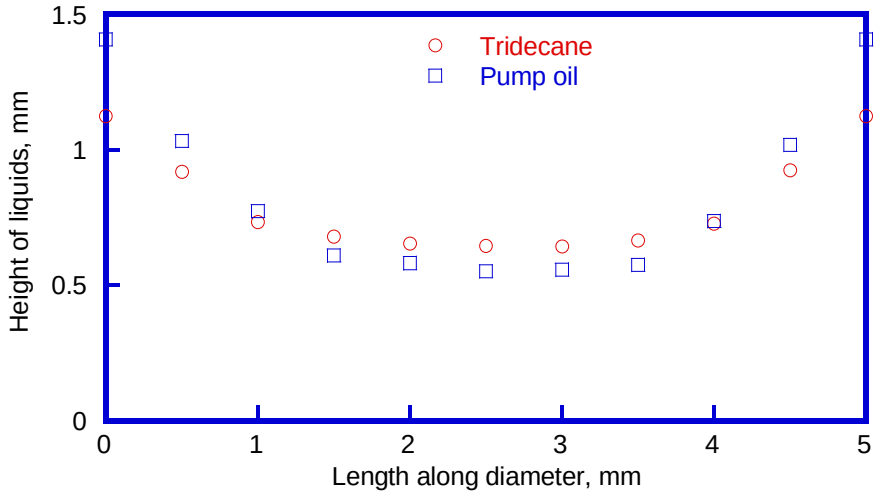

Figure 12. Superposition of the profiles of tridecane and pump oil.

Another important characteristic that can be evaluated from the profile of the liquids is the exposed surface area. This is done by revolving the fourth order polynomials around the center point (2.5 mm) and using the following equation from [33]:

$$A_s = \int_a^b 2\pi\, f(x)\, \sqrt{1 + [f'(x)]^2}\, dx \qquad (13)$$

where A_s represents the surface area of the revolution of the function f(x) between points a and b. From this method the exposed surface areas were estimated to be 24.0 mm^2 and 70.6 mm^2 for tridecane and the pump oil, respectively. These calculations represent a good estimation of the respective initial surface areas. During the evaporation the liquids evaporate uniformly over the exposed surface area until the center of the liquid completely evaporates. This portion of the sample is the first to completely evaporate because it has the least amount of substance. After the center has evaporated the liquid continues to wet the sides of the pan and begins to evaporate as a ring of liquid. Figure 13

illustrates this process of evaporation that is dependent on the exposed surface area. In this figure the dotted line represents the exposed surface of the liquid that is evaporating and the solid line is the pan. Notice how the rate of evaporation will vary based on the amount of remaining liquid through the height of the wetting liquid, h and h', and that the wetting angles, θ, θ', and θ'' should remain the same throughout the evaporation process.

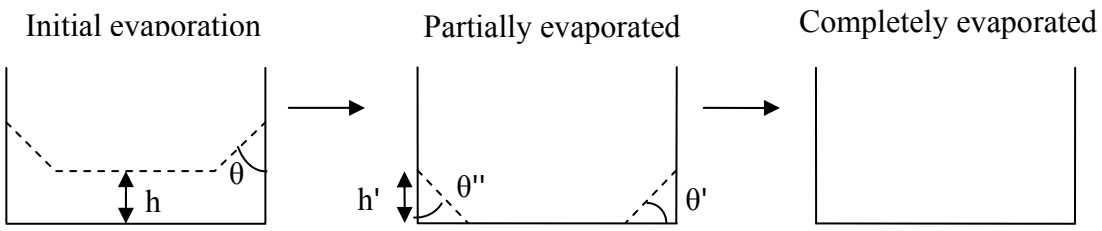

Figure 13. Evaporation process with respect to surface area.

This implies that the exposed surface area from which the liquid is evaporating is not a constant throughout the evaporation process and is instead some function of the wetting angle and the amount of liquid. Based on this analysis, the rate of evaporation will remain relatively constant until the profile of the liquid in the container resembles that of the partially evaporated state from Figure 13 and then the rate of evaporation will reduce with time until the liquid is completely evaporated. This can be accounted for if testing is stopped when the mass loss is equal to the estimated mass of the cylinder of liquid with a height of h. This is approximated by finding the volume of the cylinder of liquid and multiplying this value by the density of the sample. Once this mass has been evaporated then the partial evaporation condition from Figure 13 begins and the rate changes significantly. If the wetting angles were assumed to be constant throughout the evaporation process then the volume of the liquid that is wetting the pans will also be

constant. Using the previously calculated wetting angles and the height difference between the maximum and minimum heights of the liquid surface, the area of a two dimensional right triangle can be found from trigonometry. These triangles were then revolved around the inner surface of the pans, which resulted in the volumetric calculations of 0.16 mm^2 and 0.78 mm^2 for tridecane and the oil, respectively. Multiplying these volume calculations by the respective liquid densities results in a good estimation of the mass of the liquids contained inside the wetting regions. These masses were found to be 0.12 mg and 0.67 mg for tridecane and the oil, respectively. These masses correlate to 1.33 % and 2.39 % of the initial masses of tridecane and the oil. Since these masses are such a small percentage of the initial masses of the liquids it is very difficult to determine from the data when the partial evaporation conditions are active. Additionally, since there is so little liquid remaining in the pans at that moment and the liquid is at a relatively high temperature, near the boiling point of the substance, the remainder is evaporated very rapidly and the affect it has on the overall evaporation rate can be neglected.

Understanding how essential factors like the initial mass of the sample, surface area, heating rate of the sample, flow rate of air, and the temperature can vary between testing cycles is key for establishing repeatable testing procedures. These factors were held paramount in establishing all testing procedures. To test the repeatability of the alkane testing three undecane burn tests were compared. The results can be seen in Figure 14. The three tests experienced the same maximum temperature and were heated at the same rate. It can be assumed that all three tests had the same exposed surface area and no air flow. Since all three example runs were conducted using the same substance, the

molecular weight remained constant through testing. The factors that proved to be very cumbersome to maintain as constants through testing cycles were the initial mass and initial temperatures of the samples.

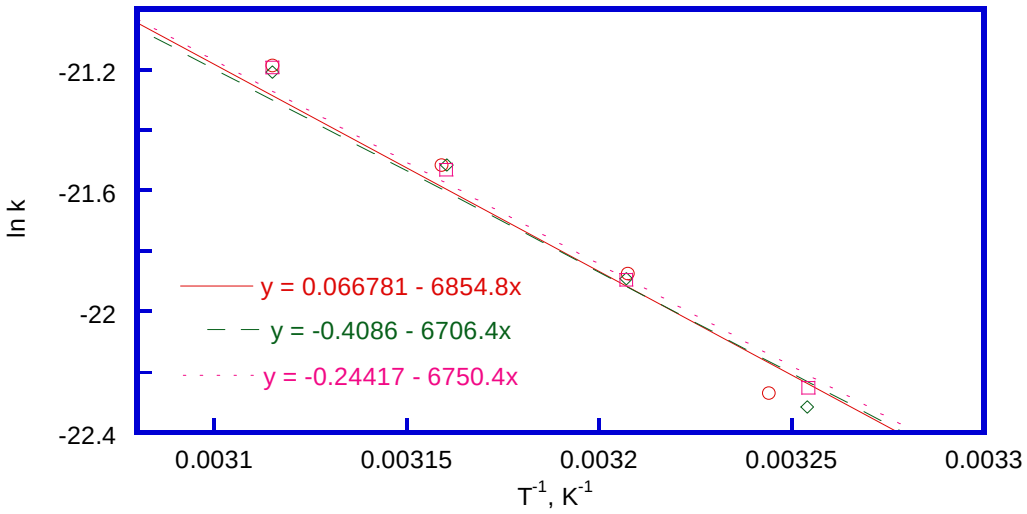

Figure 14. Repeatability results for Arrhenius Plot of undecane.

Regulating the initial masses was performed by an iterative process involving the micropipette and numerous weight measurements. An initial amount of the sample, in this case undecane, was taken from its original container by use of the micropipette. This value was then measured and recorded. The subsequent tests gained the initial mass in the same way however, if the initial mass of less than or greater than the first test by as little as 0.1 mg then an iterative process of adding and subtracting mass was conducted to gain conformity in the measurements.

The initial temperature was an easier variable to control. Essentially all the initial samples were at the same ambient room temperature, since they require no special storage conditions. The instrumentation setup used was allowed to cool to the same temperature prior to start of a new test. These initial instrumentation temperatures were

all within 0.2 °C of each other. Table 5 lists the test run and the associated initial masses (M_i) and temperatures (T_i). Additionally, Table 5 lists the pre-exponential values and the calculated activation energy values for each test run.

Table 5. Repeatability comparison results for undecane.

Undecane	M_i (mg)	T_i (°C)	A $\left(\frac{mg}{sec}\right)$	E_a $\left(\frac{kJ}{mol}\right)$
Test 1	9.19	26.3	1.1	55.8
Test 2	9.13	26.1	0.7	54.6
Test 3	9.17	26.2	0.8	54.9

Table 5 relates the importance of the initial mass and initial temperature on the calculated activation energy. From the table the lowest initial mass coincided with the lowest initial temperature, which resulted in the lowest calculated activation energy and pre-exponential constant. Likewise, the highest measured initial mass coincided with the highest initial temperature which, as expected, resulted in the highest calculated values of the activation energy and pre-exponential constant. Table 5 also demonstrates the remarkable differences in the pre-exponential constant stemming from very small changes in initial conditions. However, these variations in calculated values can be considered negligibly small and as a result the testing conducted in this investigation has been deemed valid and repeatable.

3.1.2 Static testing

Static testing, as it has been termed in this investigation, is a method of testing samples over a long period of time at the same temperature. The intent of this type of testing is to provide long isothermal periods between incremental increases and decreases in temperature to allow for distinguishing between transient changes in the evaporation

rates and actual rates at specific temperatures. As the temperature is increased and decreased the evaporation characteristics are recorded during the isothermal periods. Increases and decreases in temperature during static testing were done at a very low rate, which was programmed by the instrumentation to be 0.001 °C/min. This method of testing proved to be very effective at defining the characteristics of the alkanes at lower level temperatures (25 -75 °C). This is very important because of the very nature of static testing. With the inherent properties of the alkanes such as lower densities, molecular weights, and boiling temperatures, as compared to the pump oil, the low temperature data points were generally too scattered to retrieve any useful results from a more rapid form of testing. This is due, in part, to the fact that once the alkanes are exposed they begin evaporating and a faster heating rate results in noisy data at lower to atmospheric levels. This is why the static testing procedures were introduced; to give a more complete explanation of the evaporation rates of the alkanes for a wider temperature range. This phenomenon can better be described by comparing the static and dynamic test results for one of the alkanes. Figure 15 is such a plot of the logarithm of the evaporation rate against the inverse of the absolute temperature. The unfilled circles represents data collected from dynamic testing of hexadecane. Notice how as the temperature decreases the data points become less uniform and begin to fan out altering the slope of the linear fit line.

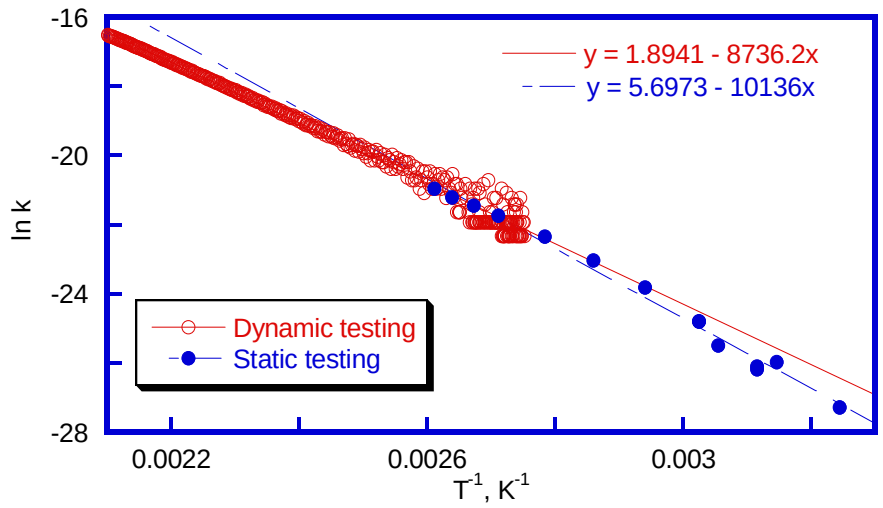

Figure 15. Static and dynamic Arrhenius Plot for hexadecane.

Since the slope of this line is directly related to the activation energy, then another means of collecting the lower temperature data is necessary for a more adequate and complete representation of the evaporation rate from room temperature and above. This makes static testing an ideal approach for collecting these data. The sample begins testing at room temperature (25 °C), where it remains for an extended period of time then it is heated to a slightly higher temperature and again held isothermal. This is repeated until a predetermined temperature, the temperature at which dynamic testing has been deemed valid (usually 60 -75 °C), is reached. This data is then recorded and analyzed by means of the Arrhenius equation, just as done with dynamic testing data. The total collection of data is then graphed in the same Arrhenius Plot and linear lines are fitted to the separate data to approximate the activation energies for low and high temperature level evaporation. This type of plot, as shown by Figure 15, provides an expected result: at lower temperatures the molecules require more energy to be broken than at higher temperatures. From Figure 15 it can be determined that the activation energy for

hexadecane is about 16.0% higher at a temperature range between 25 °C and 75 °C than at higher temperatures.

Once static testing was determined to be an appropriate means of determining the overall evaporation characteristics of the alkanes, all the alkanes were tested with this method. Figure 16 shows the resulting Arrhenius Plot for all the alkanes. There are several interesting results that can be observed in this figure. Most notably is the shifting down and to the left for the higher molecular weight alkanes. This shifting has a two part explanation. The downward shifting is representative of an increase in the activation energy of the alkanes, as can be seen in Figure 16. This is expected because as the molecular weight increases between alkanes so do some essential molecular properties.

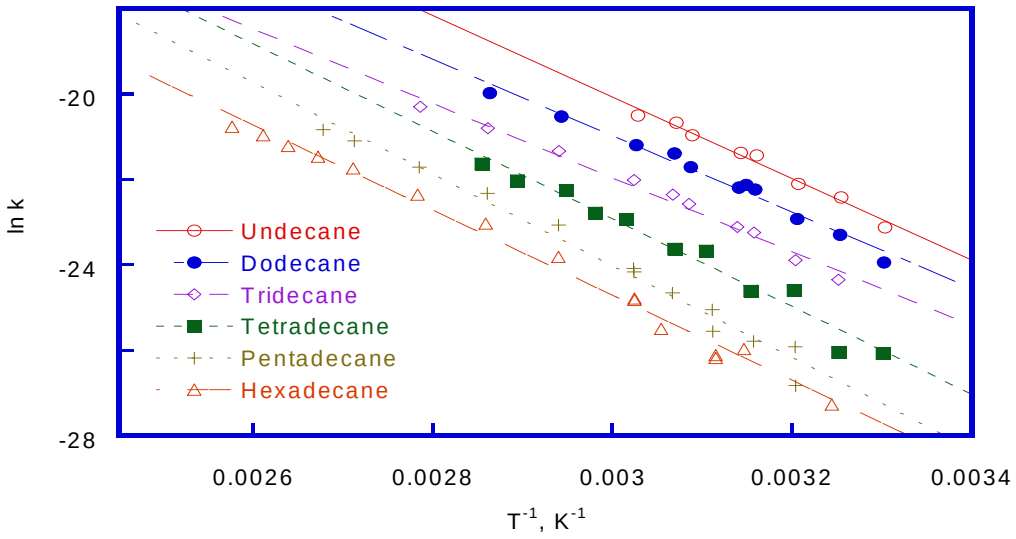

Figure 16. Static temperature testing for all alkanes.

The density, the molecular weight, and the boiling temperature all increase with ascending alkane order. As discussed earlier in this work, an increase in such material properties requires a greater energy to break the intermolecular attractions. As seen in Figure 16, the shift to the left also seems to increase with ascending alkane order. This

shifting represents an increase in the maximum temperature of the valid static testing range. In other words, the higher the alkane ranking the higher the static temperature can be recorded and remain a valid and accurate representation of the evaporation rate characteristics. The activation energies and pre-exponential constants were calculated from the linear best fit lines of the data presented in Figure 16 and the results are displayed in Table 6. It is interesting to note that all the offsets of the Arrhenius Plots were positive numbers resulting in large values of the pre-exponential constants. Also, the fact that the activation energies do not increase incrementally as expected, is rather peculiar. This could be a result of one of two things, or a combination of the two. The first possible explanation is that there are errors in the testing, from either the parameters or the testing itself. The other explanation is that the data were not isolated for the same temperature range for each alkane, but rather for the entire valid range specific to each individual alkane. This in effect alters the slope of the linear fitted line by averaging the lower temperature data with those of the more elevated temperature data. However, after creating similar plots for the truncated ranges a similar phenomenon is present. This unexpected result is ultimately explained by the sporadic nature of data obtained from static testing.

Table 6. Activation energies and pre-exponential constants for all alkanes, obtained from static testing.

Alkanes	A $\left(\frac{mg}{sec}\right)$	E_a $\left(\frac{kJ}{mol}\right)$
Undecane	5317	79.5
Dodecane	316.4	74.5
Tridecane	61.21	72.2
Tetradecane	2623	85.4
Pentadecane	3575	89.3
Hexadecane	182.9	82.9

Even though there are these unexpected fluctuations, there still are some fundamental relationships that can be learned from the static testing of alkanes. Primarily, static testing of alkanes is only valid in the low temperature range. In addition to this, the energy required to break intermolecular attractions is greater at lower temperatures. To further explain the latter relation, an averaging of the calculated values of the activation energies for higher heating rates for dynamic testing was done. These averages were then compared to the static values for the corresponding alkanes. The percentage of increase of the activation energies was then obtained for each alkane by this method. Taking the mean value of the percentage increase in activation energy for the alkanes resulted in 25.7 %. This means that, on average, the required activation energy at lower temperatures is 25% greater than what is necessary at higher temperatures. This correlates to a slower evaporation rate at lower temperatures, as can be expected. If these results were to be generalized to all liquids then it could be stated that liquids near room temperature require 25% more energy to break intermolecular attractions (evaporate) than at elevated temperatures.

Static testing of the pump oil was conducted in a similar fashion, but resulted in very different conclusions. First, due in large part of the inherent material properties of the oil static testing proved to be the only viable method of understanding how the oil evaporates. Dynamic testing, in other words, is not a valid approach for defining the evaporation of this oil. This is because rapidly heating the oil produced very little retrievable data. Also, if the heating rate and/or the maximum temperature were set too high the oil would simply burn and leave carbon deposits on the instrumentation. Therefore, static testing was preferred and for the pump oil the testing was usually over 60 hours. Testing over such a long time has several benefits and hindrances. The major benefit of testing for such a long period of time is that a lot of good usable data can be calculated. Also, long testing periods provide a chance to fluctuate the temperature to many different settings gaining a more complete estimate of the evaporation characteristics of the oil. The main negative result of such testing is in the accuracy of the instrumentation itself. When testing evaporation over such a long period of time the instrumentation used would suffer from drift. Instrumentation drift is a loss of calibration that stems from the use of the instrument. As an instrument is used it tends to become less accurate with time, hence the need for frequent recalibration. However, since testing of this type cannot be stopped to recalibrate the instrumentation; measurements must be taken continuously. To account for instrumentation drift a series of drift tests were conducted to determine to what extent the instrument was reducing in accuracy over the testing period.

For drift testing the testing procedure remained exactly the same as the normal testing. However, the aluminum pans were kept empty in the drift tests. The theory

behind this logic is that at the temperatures that were being tested the aluminum would not be losing mass, or at least not a measurable amount. Conducting these tests resulted in an observed mass loss of the empty pans on the order of 0.5 mg over a 64 hour period. The extent of this drift can be seen in Figure 17 which is a graph of the measured mass loss of the oil as compared to the drift results for two test runs. All testing experienced the same temperature controlling procedure and all other conditions were maintained as constants. Figure 17 shows a total measured mass loss for the pump oil as about 0.83 mg for the 64 hour testing. The drift testing resulted in a fictitious mass loss around 0.34 mg, which would be a significant percentage of the measured mass loss for oil. Also notice from Figure 17 that the mass loss due to drift is represented by a relatively zero sloped line until about hour 4. That is why drift corrections are not needed for the static testing of the alkanes, because they evaporated well within a few hours.

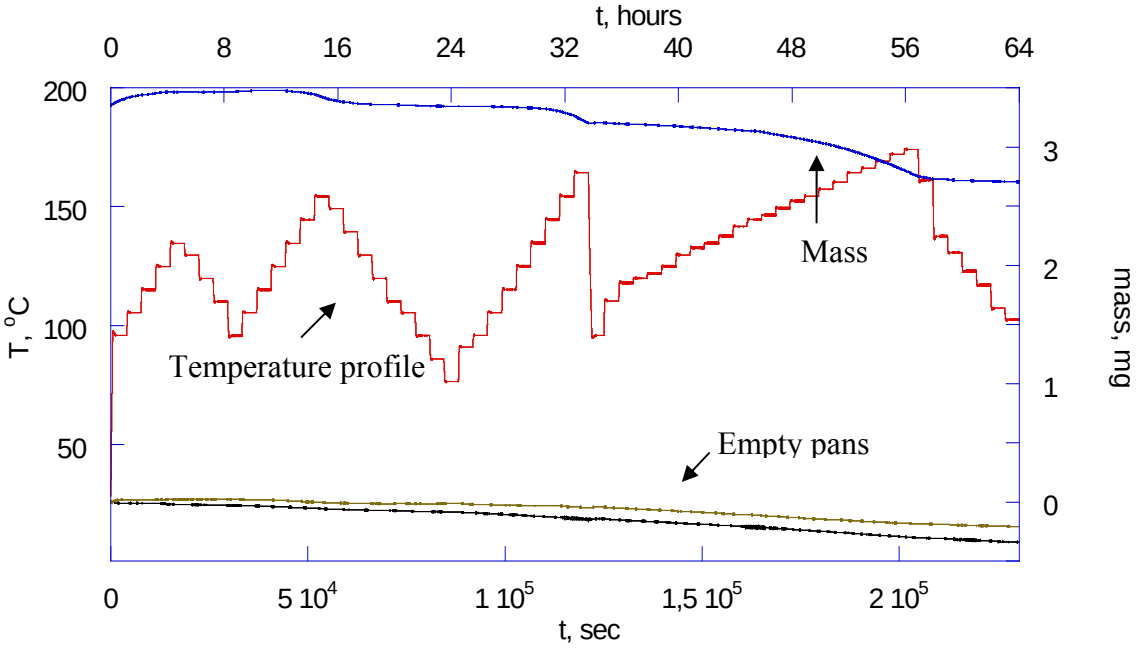

Figure 17. Drift test comparison for pump oil.

Correcting for drift is necessary prior to analyzing the data. To do this the mass loss due to drift is simply subtracted from the measured mass loss of the oil. Since the fictitious mass losses were recorded as negative values, as a result of drift test calibrations prior to testing, the magnitudes of the drift mass loss are added to that of the measured oil mass losses continuously for the entire testing period. The series of drifting tests never resulted in the exact same total mass loss, but the results were close in value and the overall shape of the mass loss curve. A function was linearly fitted to the instrument drift data and was then subtracted from the measured mass loss profile for the pump oil. The result can clearly be seen in Figure 18, in which the measured and the actual, after correction, mass losses are plotted with respect to time, temperature, and mass. Notice that the mass loss profile of the oil maintains a very similar shape but is increased in magnitude. This increase is a result of drift corrections of the measured data and accounts for the loss of calibration of the instrumentation over the complete testing cycle.

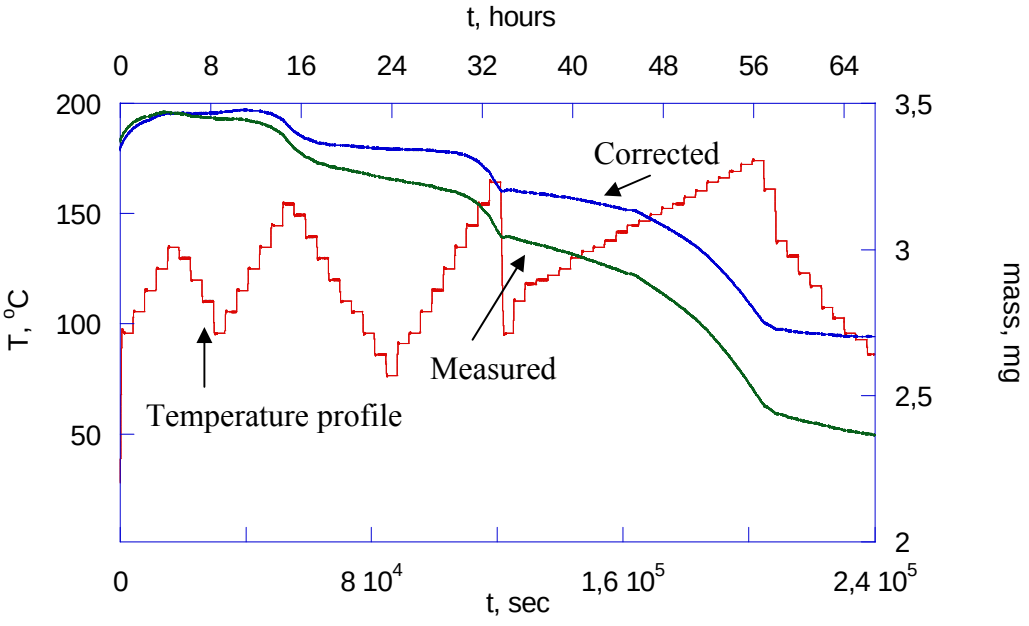

Figure 18. Drift correction for pump oil.

After the pump oil data was corrected the activation energy was then calculated. The method of calculation utilized the Arrhenius Equation and the related Arrhenius Plot for the corrected pump oil data can be seen in Figure 19. As usual a linear best fit line was drawn through the data points in order to obtain information on the slope and offset of the Arrhenius plot. From this information the activation energy of the pump oil was calculated to be 83.6 $\left(\frac{kJ}{mol}\right)$ and the pre-exponential constant to be 6.9 $\left(\frac{mg}{sec}\right)$.

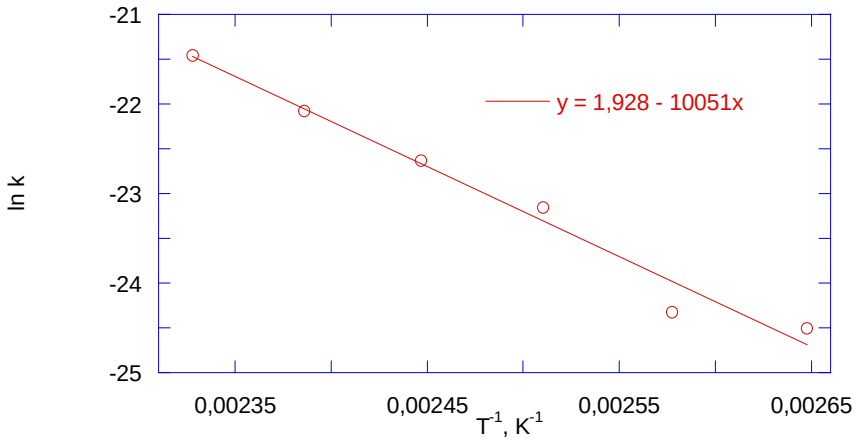

Figure 19. Arrhenius Plot of pump oil for calculating the activation energy.

3.1.3 Dynamic testing

Dynamic testing is the measurement of the mass loss of a sample with respect to time while experiencing a continuous increase in temperature. The heating rates for the series of dynamic tests were 0.5, 1, 3, 5, 10, 20, and 30 °C/min. All the alkanes were heated to a maximum temperature of 300 °C at these varying rates. Needless to say that all of the alkanes completely evaporated well before the maximum temperature was reached. In fact the testing usually lasted less than 15 minutes. As mentioned in the previous section, results from dynamic testing proved to provide stable data for higher

temperatures, generally over 60 °C. The main difference between dynamic testing and static testing is that in dynamic testing the temperature of the sample is rapidly changing allowing no time for it to stabilize in temperature. As a result, dynamic testing never has an isothermal condition. Just as in the other testing procedures the temperature and mass loss were recorded continuously throughout the testing. Likewise, the recorded data was analyzed by means of the Arrhenius Equation and were plotted to estimate the slopes and the offsets of the linear best fit lines. Figure 20 is such a graph, displaying the collected data and the linear fitted curves to that data for all the alkanes. There is once again a pattern of shifting between the alkanes. Figure 20 shows a distinct shift downward and to the left for ascending alkanes. The shifting in the downward direction is an expected result as it represents an increase in the required activation energy to break intermolecular bonds in the increasing order of such properties as molecular weight and boiling point. As in static testing the shifting to the left is related to the valid temperature range of the data. Although all the alkanes were tested under the same conditions and experienced the same temperatures, the amount of scatter in the lower temperature data varied between the alkanes. From Figure 20 it can be deduced that the lower the melting point, for instance, the better the low temperature data. Here better refers to data that is more consistently repeatable and is more uniform for temperatures less than 60 °C. Also notice in Figure 19 that the Arrhenius Plots for dodecane and tridecane are almost on top of each other, whereas the other alkanes have more significant spacing between them. This could be because of all the alkanes, dodecane and tridecane have the closet tabulated values of boiling point, density and molecular weight.

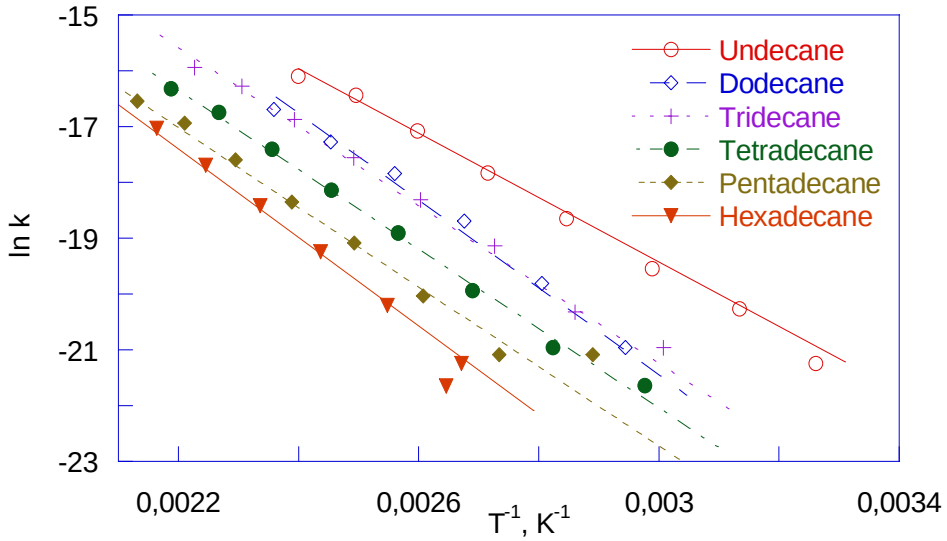

Figure 20. Dynamic temperature testing for all alkanes.

Tables 7, 8, and 9 display the resulting calculations derived from Figure 20. Each table lists the alkane tested and the associated activation energy calculated from the Arrhenius equation. Additionally, the heat of vaporization was calculated by means of the Antoine equation for comparative purposes. Table 7 has been compiled from data collected at the lowest acceptable heating rate, 10 °C/min. Acceptable in this case is defined by a heating rate that gives consistently repeatable results. Table 8 represents the data collected from a 20 °C/min heating rate and Table 9 was made from the data measured with a 30 °C/min heating rate. These tables show that the measured values for each alkane are in close proximity to each other, within 3-4 $\left(\frac{kJ}{mol}\right)$. Similarly, the theoretical values of the heat of vaporization from the Antoine's Equation are within a similar range for each alkane. Notice from the three tables and comparison of the two calculation methods reveals good agreement.

Table 7. Comparing Arrhenius to Antoine Equation results for a heating rate of 10 °C/min.

Alkanes	Ea $\left(\frac{kJ}{mol}\right)$	ΔH $\left(\frac{kJ}{mol}\right)$
Undecane	52.67	52.01
Dodecane	54.04	53.67
Tridecane	54.55	53.17
Tetradecane	57.06	59.57
Pentadecane	79.31	78.90
Hexadecane	73.39	74.46

Table 8. Comparing Arrhenius to Antoine Equation results for a heating rate of 20 °C/min.

Alkanes	Ea $\left(\frac{kJ}{mol}\right)$	ΔH $\left(\frac{kJ}{mol}\right)$
Undecane	52.95	52.08
Dodecane	56.10	57.75
Tridecane	54.91	56.46
Tetradecane	51.27	53.00
Pentadecane	73.81	77.38
Hexadecane	67.45	69.75

Table 9. Comparing Arrhenius to Antoine Equation results for a heating rate of 30 °C/min.

Alkanes	Ea $\left(\frac{kJ}{mol}\right)$	ΔH $\left(\frac{kJ}{mol}\right)$
Undecane	51.78	51.22
Dodecane	54.40	56.83
Tridecane	55.14	54.16
Tetradecane	52.60	54.42
Pentadecane	67.99	68.99
Hexadecane	70.33	71.72

The mean values of the activation energies and pre-exponential constants were determined for all testing of higher heating rates, 10 °C/min and greater. Since dynamic testing proved to be more consistently repeatable, these mean values are very good representations of the actual values. The resulting values can be seen in Table 10, which have been estimated with a reliability of 95%.

Table 10. Average activation energies and pre-exponential constants for all alkanes.

Alkanes	E_a $\left(\frac{kJ}{mol}\right)$	A $\left(\frac{mg}{sec}\right)$
Undecane	52.5 ± 0.74	0.46 ± 0.11
Dodecane	54.8 ± 1.32	0.45 ± 0.19
Tridecane	54.9 ± 0.36	0.22 ± 0.04
Tetradecane	53.6 ± 3.64	0.12 ± 0.12
Pentadecane	70.9 ± 4.95	9.25 ± 10.46
Hexadecane	70.4 ± 3.57	4.35 ± 4.01

In addition to the mentioned statistical analysis of the measured data, an error analysis of the instrumentation was also conducted. The instrumentation used for the testing, as mentioned in the testing procedure section of this work, was found to be very precise.

The propagation of errors from the measured variables of mass and temperature to the calculation of the activation energies is as follows. It was first noted that the activation energy can be written as a function of both the mass and temperature of the sample. The following empirical equation was used:

$$E_a(m,T) = -RT\ln\left|\frac{\left(\frac{m}{t}\right)}{A}\right| \quad (14)$$

where the ratio of mass, m, to time, t, represents the rate of evaporation is kg/sec, T is the absolute temperature, R is the gas constant (8.314472 J mol^{-1} K^{-1}) and A is the pre-exponential constant found from the previously presented Arrhenius equations. Using this equation in association with the chain rule in order to obtain the maximum possible error in the activation energy provides:

$$\delta E_a = \left|\frac{\partial E_a}{\partial m}\,\delta m\right| + \left|\frac{\partial E_a}{\partial T}\,\delta T\right| \quad (15)$$

which can be simplified as:

$$\delta E_a = m\,\delta m + T\,\delta T \quad (16)$$

which m and T are the measured masses and temperatures, respectively and δm and δT are errors associated with the mass and temperature measurements. The mass error was found to be 0.001 mg and the temperature error was found to be 0.3 °C. This means that a mass measurement of m and a temperature measurement of T will result in the recorded values of m ± 0.001 mg and T ± 0.3 °C, respectively. These errors will propagate through to the calculation of the activation energy and as a result must be accounted for. It should be noted that the error resulting from temperature measurements dominates the total propagated error for the activation energy, thus the mass error could be neglected for simplicity, but was not in the following error analysis. Equation (14) was used to

calculate the activation energy as a function of mass and temperature. Then equation (16) was used to calculate the instrumentation error inherent to the calculation of the activation energy, also as a function of mass and temperature. The ratio of these errors to that of the activation energies were taken to provide the percentage error. This was done for all the alkanes for both the static and dynamic testing regimes. The resulting maximum percentage errors and activation errors for all alkanes and both testing regimes can be seen in Table 11. Notice that as it was related in the procedure section of this work the precision of the testing equipment was found to be very high and resulted in a range of estimated instrumentation errors of 013 – 0.30 %.

Table 11. Propagated errors of the activation energies for all alkanes.

Alkanes	Static Testing		Dynamic Testing	
	$E_a \left(\frac{kJ}{mol}\right)$	$\frac{\delta E_a}{E_a}$ (%)	$E_a \left(\frac{kJ}{mol}\right)$	$\frac{\delta E_a}{E_a}$ (%)
Undecane	79.5 ± 0.11	0.135	52.5 ± 0.13	0.253
Dodecane	74.5 ± 0.11	0.152	54.8 ± 0.15	0.268
Tridecane	72.2 ± 0.12	0.162	54.9 ± 0.16	0.285
Tetradecane	85.4 ± 0.11	0.133	53.6 ± 0.16	0.300
Pentadecane	89.3 ± 0.12	0.137	70.9 ± 0.15	0.210
Hexadecane	82.9 ± 0.13	0.152	70.4 ± 0.18	0.255

3.2 Mixtures testing

A series of testing cycles that were not of pure alkanes but rather a mixture of them were conducted and rightfully termed mixtures testing. The procedures for these tests were the same as the dynamic testing previously described. However, the only difference was in the samples being tested. Mixture testing consisted of taking equal

volumetric portions of two separate alkanes and thoroughly mixing them in a beaker. Once these alkanes were mixed the 50-50 mixture was then transferred from the beaker to the aluminum testing pans via the micropipette. The data was then processed as before using the Arrhenius Equation and constructing the plots. Figure 21 and 22 are two Arrhenius Plots constructed from the mixture data for a heating rate of 20 °C/min and 30 °C/min, respectively. In both plots it is easy to see that there is very little spacing between mixtures, unlike what was observed for pure substances. It also seems that regardless of heating rate the mixtures exhibit evaporation characteristics that most closely resemble that of pure undecane. A resulting hypothesis is that the molecularly lighter substance evaporates first. That is except for the undecane and tridecane mixtures. The slopes of these linear fitted lines are significantly below that of pure tridecane and, to a lesser extent, below that of pure undecane. This specific mixture seems to reduce the required activation energy needed to overcome intermolecular attractions below that of the values calculated for the pure components of the mixture.

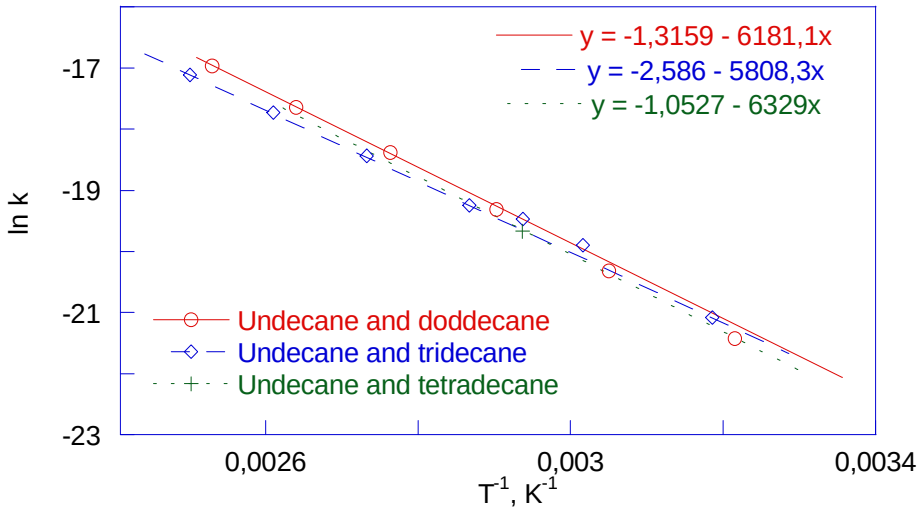

Figure 21. Arrhenius Plot of specific mixtures heated at a rate of 20 °C/min.

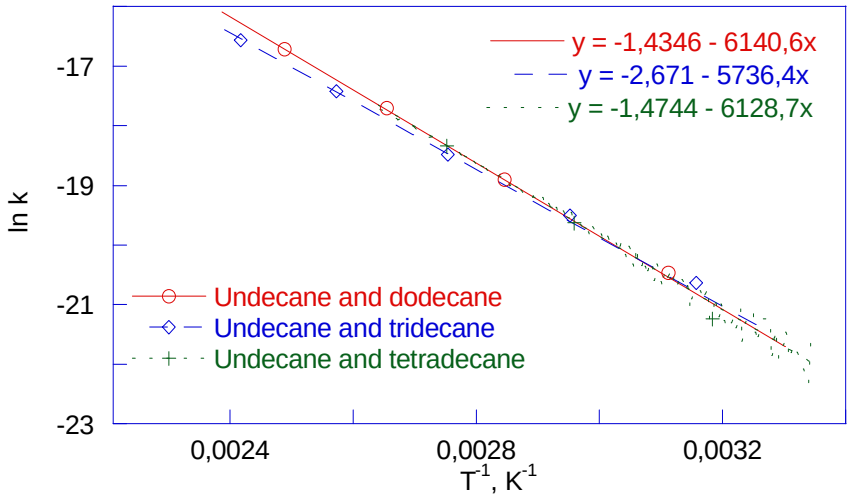

Figure 22. Arrhenius Plot of specific mixtures heated a rate of 30 °C/min.

To further elaborate on the results of alkane mixtures Tables 12 and 13 have been constructed. These tables present the calculated activation energies and pre-exponential constants for both pure testing and of mixtures. Included in the mixture data are the averaged values of the activation energies and pre-exponential constants between the two pure substances found in the specific mixtures. The second values, after the commas, are these averaged calculations. Table 12 represents data retrieved from the 20 °C/min testing and Table 13 was constructed from the 30 °C/min data.

Table 12. Comparison between mixtures and pure alkanes heated at 20 °C/min.

Alkanes	Ea $\left(\frac{kJ}{mol}\right)$	A $\left(\frac{mg}{sec}\right)$
Undecane	52.95	0.54
Dodecane	56.10	0.63
Tridecane	54.91	0.23
Tetradecane	51.27	0.05
Un & Do mix	51.39, 54.53	0.27, 0.59
Un & Tri mix	48.29, 53.93	0.08, 0.39
Un & Tetra mix	52.62, 52.11	0.35, 0.30

Table 13. Comparison between mixtures and pure alkanes heated at 30 °C/min.

Alkanes	Ea $\left(\frac{kJ}{mol}\right)$	A $\left(\frac{mg}{sec}\right)$
Undecane	51.78	0.37
Dodecane	54.40	0.37
Tridecane	55.14	0.26
Tetradecane	52.60	0.07
Un & Do mix	51.06, 53.09	0.24, 0.37
Un & Tri mix	47.70, 53.46	0.07, 0.32
Un & Tetra mix	50.96, 52.19	0.23, 0.22

Comparing the tabulated values in Table 12, the following observations are made: the calculated values of the activation energy of the undecane-dodecane and undecane-tetradecane mixtures are close to the originally calculated value of pure undecane, so it seems that the earlier stated hypothesis, that the molecularly lighter substances evaporates first, has some merit. However, the undecane-tridecane mixture resulted in a reduced activation energy that is less than that of pure undecane. The undecane-dodecane and undecane-tetradecane mixtures also have close approximations with the average

activation energies of the pure substances. It should, however be noted that the undecane-tetradecane has the closer estimate to the calculated average of activation energy. This mixture also has a close approximation between the calculated and averaged values of the pre-exponential constant. The undecane-dodecane mixture resulted in a value of the pre-exponential constant that is roughly half of the average value and the undecane-tridecane mixture resulted in a value closer to $\frac{1}{5}$ the average.

Comparing the results presented in Table 13 shows similar results. Both the calculated values of the undecane-dodecane and the undecane-tetradecane mixtures resulted in activation energies close to that of pure undecane, whereas the undecane-tridecane mixture resulted in a reduced value of the activation energy, below that of pure undecane. Undecane-dodecane and undecane-tetradecane mixtures also resulted in reasonably close approximations of both the activation energies and pre-exponential constants to that of the average values. On the other hand, the values calculated for the undecane-tridecane mixture were less than that of the average activation energy and average pre-exponential constant.

From this analysis the following conclusions are made: a mixture of alkanes will reduce the activation energy needed to break intermolecular attractions and the pre-exponential constant. The extent of this reduction depends on the properties of the components of the mixture and the proportion of the mixture. It can be generalized that the reduction of the activation energy is dominated by the component of the mixture that has the weaker intermolecular bonds. That is, the mixture resultant values will most closely resemble that of the component with the lower boiling point, density, and molecular weight. This proves the hypothesis that the molecularly lighter substances of a

mixture will evaporate first. The change in the pre-exponential constant for mixtures is much more significant than that of the activation energies. While in some cases the activation energy of a mixture can be roughly estimated as the average of the components, this is not always true and large errors can result from averaging. Since the change in the pre-exponential constant is greater with mixtures this rule is even more applicable for these calculations.

Another important observation that should be made from these two figures is the dramatic difference in the reported values of the pre-exponential constants between the static and dynamic testing. The pre-exponential constant, often referred to as the frequency factor, is directly related to the frequency of the rate of the reaction. The frequency factor is equal to the collision frequency multiplied by the steric factor. The steric factor is the ratio of the observed frequency factor to that of the calculated collision frequency. Therefore, the frequency factor, or the pre-exponential constant, is proportional to the collision frequency, which represents the average number of collisions between reacting molecules for a unit of time. This implies that for static testing there are significantly more molecular collisions during evaporation than that which is observed for dynamic testing.

3.3 Microchannel evaporation testing

With the increasing popularity of MEMS devices, testing was also conducted to measure the evaporation rate of the pump oil in simulated micro-fluidic channel. These microchannel tests were designed using all aluminum parts, which consisted of a cylindrical reservoir and either a screw threaded or non-threaded plug for the reservoir.

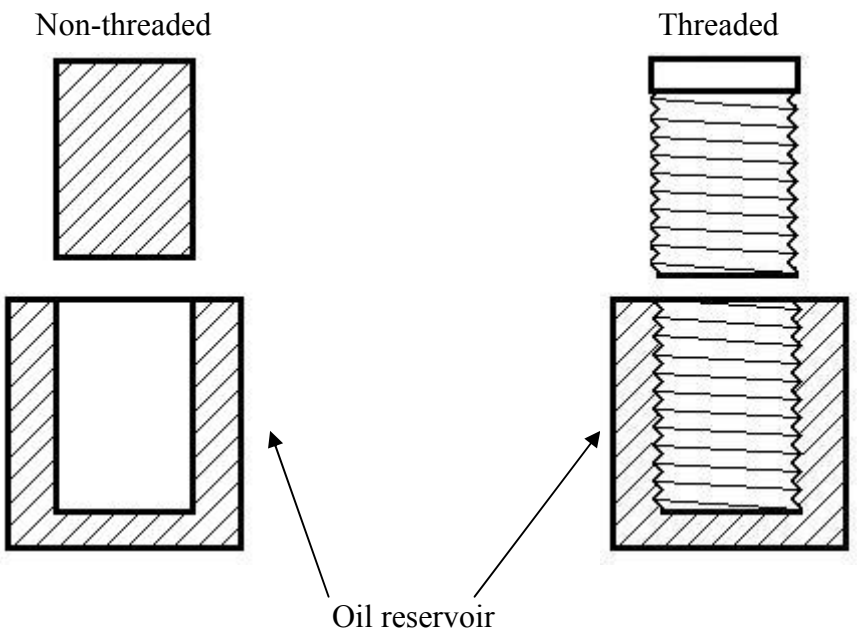

Figure 23. Pictorial representation of microchannel testing fixtures.

Figure 23 is a dimensionless pictorial representation of the design of the testing fixture used to simulate micro-fluidic channels. On the left side of Figure 23 is the non-threaded microchannel which is a mating pair of smooth aluminum cylinders. The pump oil is first put into the reservoir and then the plug is pressed into the reservoir. This limits evaporation to only a thin ring of exposed oil at the top of the reservoir. On the right side of Figure 23 is an illustration of the threaded microchannel simulation. In this setup the oil is again put inside the reservoir and the plug is set into place within the reservoir. However, in this setup the plug has external threads and the reservoir has internal threads. After the oil is in place, the plug is threaded into the reservoir. This limits the evaporation to only a small opening at the top of the reservoir, unlike the non-threaded setup, but in this design the evaporating oil has to move through the mating threads which is analogous to a micro-fluidic channel.

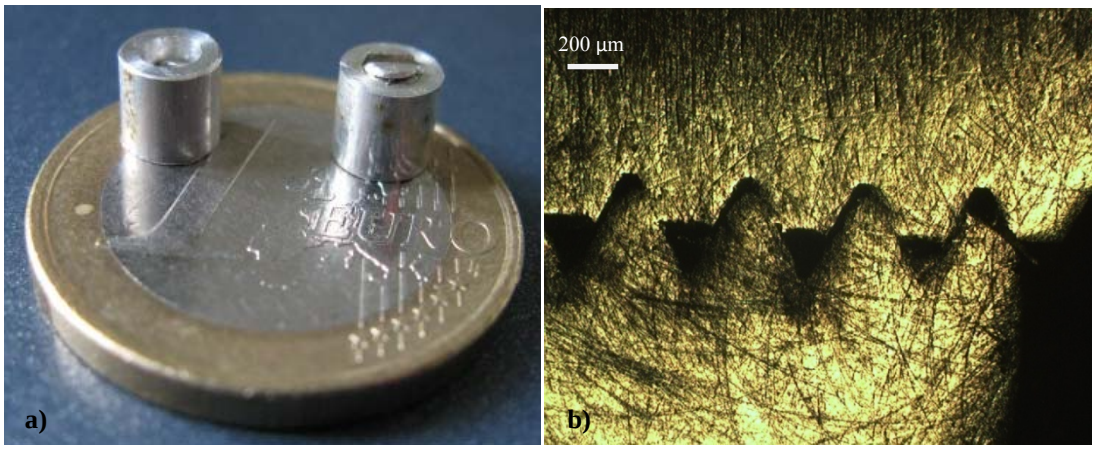

Figure 24. Microchannel fixtures: a) Relative sizes; b) Micrograph of a cross-section showing the microchannel dimensions.

Figure 24a shows both of the microchannel setups and relates the relative size of the designs as compared to a 1 Euro coin. Figure 24b is a picture of a cross sectional cut of the threaded design. As mentioned, this design simulates micro-fluidic channels and can be seen in Figure 24b, which shows an equilateral triangular channel with a 200 µm side.

These two designs were utilized to gain a better understanding of the nature of evaporation from micro-fluidic channels. The actual testing followed the same procedure as for the static testing of the pump oil described in a previous section of this work. The collected data was then analyzed, as before, using the Arrhenius Equation to calculate the activation energy and pre-exponential constant for the two setups. Figure 25 is the Arrhenius Plot for both conditions with a linear best fit through the data for each. As seen in Figure 25, the threaded design has a much steeper slope than that of the non-threaded design and as a result is expected to have higher activation energies. The subtle differences of these designs produced dramatically different offsets between the two and this would correlate to very different values of the pre-exponential constants. Calculating for these values results in an activation energy of 55.8 $\left(\frac{kJ}{mol}\right)$ and 104.5 $\left(\frac{kJ}{mol}\right)$, for the

non-threaded and threaded designs, respectively. Likewise, the pre-exponential constants were found to be respectively 1e-4 Hz and 30.8 Hz for the non-threaded and threaded designs.

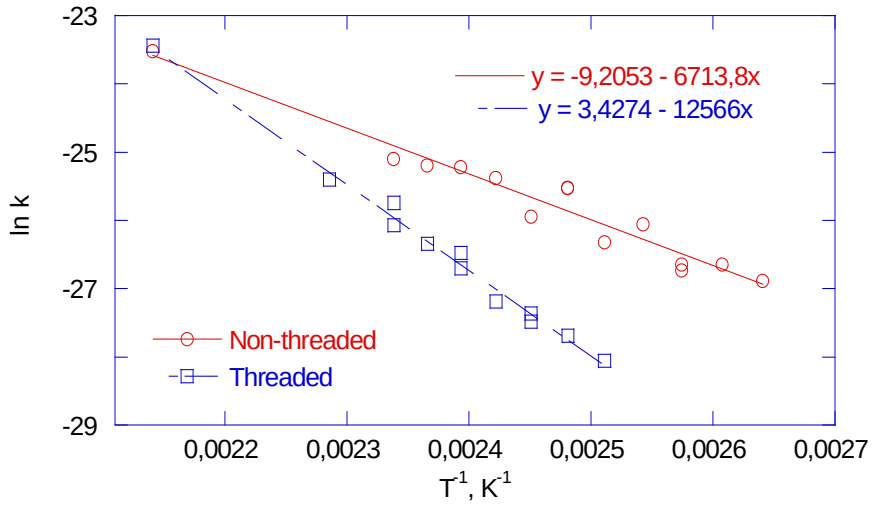

Figure 25. Arrhenius Plot for both threaded and non-threaded microchannels.

As expected, the required activation energy to break intermolecular attractions of the pump oil while in a threaded microchannel is much greater than the previously tested open surface. However, the non-threaded microchannel the required activation energy is much less than that of the open surface and is in fact less than the open surface that is exposed to a 25 mL/min flow rate of air. This created many questions during analysis and to help explain what is happening a comparison graph of the actual evaporation rates was constructed. Figure 26 is a plot of the evaporation rate (kg/s) of the threaded and non-threaded microchannel designs against the temperatures (°C) that the samples were exposed to. The data collected during testing was fitted with exponential equations which are provided in Figure 26. The overall slope of the non-threaded design is much steeper

than that of the threaded one relating that the non-threaded design evaporates much faster.

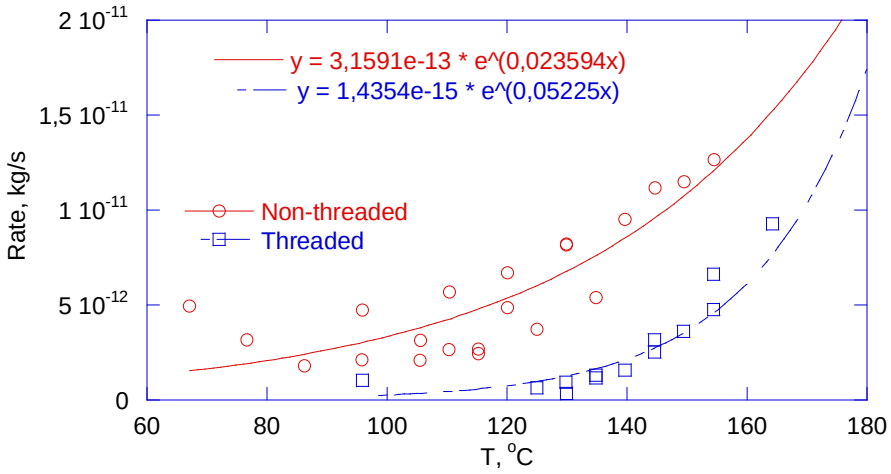

Figure 26. Rates of evaporation for threaded and non-threaded microchannels.

After an examination of Figure 23 it should be clear that the threaded microchannel did not begin to evaporate until the temperature had reached almost 100 °C. This is an expected result because the pump oil did not begin to evaporate until similarly elevated temperatures and the microchannel has a dramatic reduction of exposed surface area. So the same is true for the non-threaded microchannel, but the data provides different results. The reason for this is because as the non-threaded plug rests in the reservoir it displaces the oil and pushes it up along the sides of the reservoir. In addition to this displacement there are capillary forces that can generally be quite significant at these small scales and add to the displacing force of the plug. This condition has been theorized to create a pooling effect of the oil on top of the plug greatly increasing the exposed surface area from what is expected. This layer of oil on top of the plug then evaporates as in the case of an open surface, but this surface area is greater than that of the aluminum

pans used previously. Therefore, the most reliable and representative data of an actual microchannel is that of the threaded design.

CHAPTER 4

SUMMARY AND FUTURE WORK

4.1 Summary

The evaporation characteristics have been investigated for alkanes and a pump oil. Understanding how a substance will evaporate can be very useful for comparative purposes for the selection of the best lubricant for particular applications. It is possible to measure both the evaporation rate and the activation energy directly. Either of these qualitative results can be used as a comparative tool between different substances. The study of the six alkanes resulted in activation energies between 50 and 70 $\left(\frac{kJ}{mol}\right)$, whereas the pump oil investigation yielded results closer to 84 $\left(\frac{kJ}{mol}\right)$. These values are a result of dynamic testing, which produces lower and more consistent calculations of the activation energies of the alkanes. The alkanes were found to have activation energies between 72 and 89 $\left(\frac{kJ}{mol}\right)$, for static testing. The pre-exponential constant changed even more significantly between testing procedures. Static testing yielded pre-exponential constants on the order of several kHz, while dynamic testing resulted in values were in the mHz range. This means that there is a higher frequency of molecular collisions during static testing than for dynamic testing. Evaporation was also analyzed for pump oil in an air flow of 25 mL/min. The resulting calculation of the activation energy turn out to be 59.6

$\left(\frac{kJ}{mol}\right)$, which as expected is a less than the values calculated without an air flow. Additionally, a study of the evaporation rate of the pump oil in a microchannel was conducted and resulted in an activation energy of 104 $\left(\frac{kJ}{mol}\right)$. The factors that contribute most to variation of the calculation of these results are the exposed surface area, the heating rate, the flow rate of air, and of course the substance properties themselves such as density, molecular weight and boiling point. It was observed that a mixture of equal proportions of alkanes did not consistently result in the averaging of the evaporation rates. This is because the change in composition is not directly proportional to the change in the entropy of the liquid mixture. The testing helped to prove the theory that in a mixture of alkanes the molecularly lighter substance will evaporate first resulting in calculations close to a pure sample of the lighter substance. Future investigations should be conducted to gain a further understanding of the importance of the roles that different factors have on evaporation. From this added information modeling of evaporation is possible and could provide a quick comparative tool of the evaporation of new lubricants.

4.2 Modeling

The modeling of the rate of evaporation can be very cumbersome because of such non-constant contributors like the surface area which can significantly change with time. Once a specific model has been established it is only valid for the conditions examined during the derivation of the model. For this reason the modeling of evaporation must be generalized and take into account such factors. This type of modeling is discussed further in this section by means of four different approaches. These models are derived from similar setups as used in this work, specifically the surface evaporation of a sample inside

an open ended container. For the investigation and modeling of evaporation for droplets see [34-37].

Beverley et al. [38] measured and derived subsequent models for pure liquids with a range of vapor pressures (0.1 – 500 Torr). Liquid samples were investigated while partially filling an open ended cylinder that was encompassed by a vertical flowing gas stream. The actual evaporation rates were measured as the amount of mass loss from the container per unit time.

First they determined the theoretical maximum rate at which the liquids could evaporate. This is accomplished by neglecting such hindering factors as the stagnate layer of gases that forms on the surface of an evaporating liquid inhibiting evaporation. Also the liquids were assumed to be in constant equilibrium, that is, the number of molecules that are hitting and condensing on the surface of the liquid is equal to the number that is evaporating. From this the theoretical maximum evaporation in a vacuum is:

$$J_{\max} = \frac{\mathrm{P}}{\sqrt{2\pi \mathrm{MRT}}} \tag{17}$$

where P is the vapor pressure of the liquid, M is the molecular weight of the liquid, R is the gas constant, and T is the absolute temperature. The units of the evaporation flux, J_{max}, are $\left(\frac{mol}{secm^2}\right)$; which relates the number of moles of a liquid evaporating per second per area of exposed liquid surface. Understanding that the maximum can never be reached in practice, a better representation of the real evaporation process was derived.

Building from the theoretical maximum Beverley et al. conducted tests intended to measure the initial evaporation rates, where the height of the stagnate gaseous layer remains constant, and of more volatile liquids, where this height increases with time. The following relationship between the mass, m, and time, t, is:

$$t = \frac{RTh_t}{MADPz}(m_0 - \mathrm{m}) - \frac{\mathrm{RT}}{2\rho \mathrm{MA}^2\mathrm{DP}}(m_0^2 - \mathrm{m}^2) \quad (18)$$

where m_0 is the initial mass of the liquid at time zero, h_t is the total inner height of the sample tube, ρ is the density of the liquid, D is the vapor diffusion coefficient, A is the surface area of the liquid, and z is the correction factor. This model accounts for variations in the evaporation rates of liquids and has been used to determine these evaporation rates with an accuracy of a few percent.

Pichon et al. [39] have studied the evaporation of organic pollutants and have formulated a model describing the rate. The testing method was accomplished by means of thermogravimetric analysis and takes into account the effect of temperature, total external pressure, and heating rates. Testing was conducted with a constant flow of Nitrogen, in a temperature range of 20 – 800 °C, and with varying heating rates. The model itself is a mathematical representation of non-isothermal evaporation.

It was observed that the density of the flux of the pollutants, j_{fl}, was non-uniform on the surface of the liquids. This lead to the evaluation of the rate of evaporation, k, for the entire surface of the liquids to be:

$$\mathrm{k} = \int_0^R 2\pi r j_{fl} \mathrm{dr} \quad (19)$$

where r is the radius of the container and the integration is taken from the center of the container, where r is zero, to the outer edge , where r is the maximum value R.

The authors note that in this model accuracy depends on the accuracy of the liquid surface area measurement. The calculated areas and what have been termed as adjusted areas differed 20 – 30 %, generally, but can be as much as 148 % [39]. Even though these variations in the calculation of the surface area were significant, the observed and predicted values of the evaporation rates were within 10 % of each other.

Xia et al. [40] studied the evaporation rates of liquid n-alkane films. This investigation was of the thermodynamic, structural, and compositional properties of surfaces and interfaces of complex liquids. This investigation was carried out to gain a better understanding of the molecular mechanisms associated with interfacial phenomena. The data of this work was obtained by analyzing liquid films on crystalline substrates.

The model of this approach stems from the Hertz-Knudsen-Langmuir equation for the net evaporation rate [41]. It is an application of the transition state theory, which showed good agreement with experiments. Making certain assumptions the transition state theory provides the following expression to describe the evaporation rate:

$$k = \kappa \left(\frac{M}{2\pi RT}\right)^{\frac{1}{2}} \frac{RT}{N_A v_f e} \frac{Q_i^+}{Q_i} e^{\frac{-E^+}{RT}} \tag{20}$$

where κ is the transmission coefficient, N_A is Avogadro's number, v_f is the free volume per molecule in the liquid, Q_i and Q_i^+ are the partition functions for internal degrees of freedom of a molecule in the liquid and activated complex, respectively, and E^+ is the activation energy for evaporation. The authors often made the following two simplifying assumptions while applying this model: (1) the molecular degrees of freedom are unaffected in the transformation from the liquid phase to the transition phase, Q_i and Q_i^+ are equal, and (2) $E^+ = E_v$, which identifies the activation energy of evaporation with the energy of evaporation.

This approach yielded many results including the knowledge that molecular evaporation mechanisms are cooperative and sequential in nature. Evaporation was also determined to be accompanied by marked molecular conformational changes. Another important conclusion made by these authors is that the energy required to transport a molecule inside the liquid to the liquid-to-vapor transitional region accounts for a

significant amount of the total energy required to transport a molecule inside the liquid to the vapor state.

Stiver et al. [3] presents three separate models for determining the rate of evaporation of spilled hydrocarbons and petroleum mixtures. The three methods are tray evaporation, gas stripping, and distillation. Tray evaporation is the evaporation from the surface of a liquid and since it is the approach most alike to that previously discussed, it is the only configuration deemed appropriate. In this configuration the sample liquid is placed into a tray, ensuring uniform thickness, and the weight of the tray is continuously monitored. The tray itself is placed inside a wind tunnel and air is passed over the liquid at a known and/or measured rate. From this configuration the rate of evaporation can be determined by the following expression:

$$k = \frac{\kappa a P}{RT} \tag{21}$$

where P is the vapor pressure of the liquid (Pa), a is the area of the spilled liquid (m^2), κ is the mass transfer coefficient under the prevailing wind conditions $\left(\frac{m}{sec}\right)$, and k is the molar flux of the liquid $\left(\frac{mol}{sec}\right)$.

This technique and associated model has been described as ideal for measuring the rate of evaporation of crude oils by the authors. The authors also note the biggest hurdle that must be overcome when analyzing the evaporation rates of crude oils and hydrocarbons is linked to multi-component systems. Multi-component systems, also known as mixtures, are inherently difficult to express the vapor pressure as a function of the changing composition of the mixture. Even with this hindrance the authors have reported good agreement between predicted and observed rates of evaporation.

The data collected from testing can be used to compare models and to provide valuable information on the actual evaporation rate of the sample substance. The raw data includes continuous measurements of the mass of the sample. If the derivative of these data were taken with respect to the recorded time then the result is a series of data accounting for the amount of mass loss per time. This is the best representative of the rate of evaporation for a substance under the conditions of the tests. The evaporation rate is expected to change with changing temperature, and the form of the relationship of the rate of evaporation to the temperature of any given substance can be assumed to have the form:

$$\frac{dR}{dT} = \alpha R \tag{22}$$

where α is a constant of proportionality. Equation (19) is both separable and linear in the following form:

$$\frac{dR}{dT} - \alpha R = 0 \tag{23}$$

Multiplying both sides of the equation by the integrating factor of $e^{-\alpha T}$ gives:

$$\frac{d}{dT}[e^{-\alpha T}R] = 0 \tag{24}$$

Integrating both sides of the equation (21) and rearranging to a more convenient form yields:

$$R(T) = \beta e^{\alpha T} \tag{25}$$

Graphing the evaporation rates against the temperature reveals that this assumed form of the relationship of the evaporation rate with respect to temperature is valid and the values of β and α can be found from such a graph. The evaporation rates for all of the alkanes can be seen in Figure 27. The data points in this figure have been exponentially fitted and

the associated equations are included to provide estimations of the α and β values for each alkane. As can be expected, the slope of these lines increase with an increase in temperature. The changes in the slopes are also more dramatic at higher temperatures for the molecularly lighter substances.

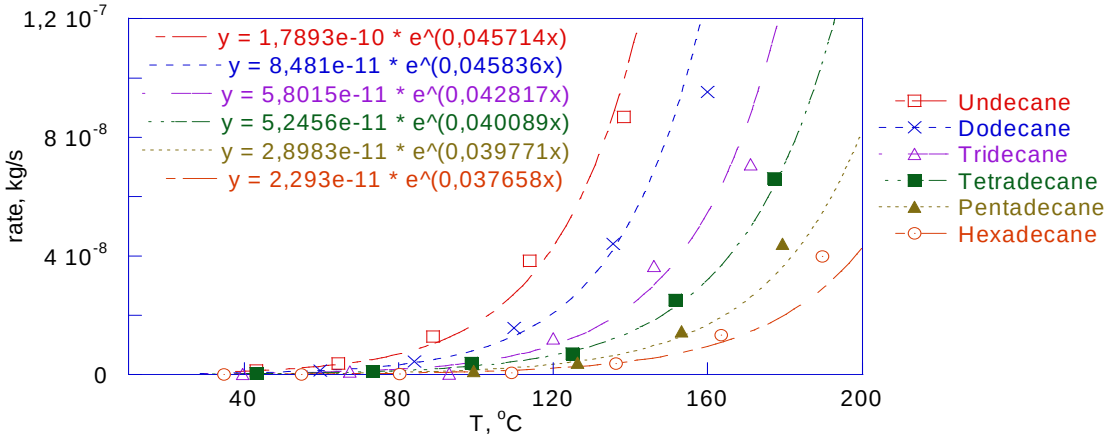

Figure 27. Measured evaporation rates versus temperature for all alkanes.

These evaporation rates can be compared to the theoretical maximum rates of evaporation for comparative purposes. The theoretical maximum evaporation rate was derived from evaporation in a vacuum and has been calculated from equation (14). This equation provides an estimate of the molar flux and must be multiplied by the surface area, the molecular weight of the substance, and a conversion factor to change the units to kg/s. The surface area was previously determined to be 24 mm^2, or 2.4e-5 m^2, and the molecular weights of the alkanes have been tabulated in an earlier section. Figure 28 presents the results of the calculation of the maximum evaporation rates of all the alkanes. This is similar to Figure 24, however the rates are much greater than what was

recorded from experimentations. Note that the theoretical maximum rate of evaporation for hexadecane is close to the measured value of evaporation rate of undecane.

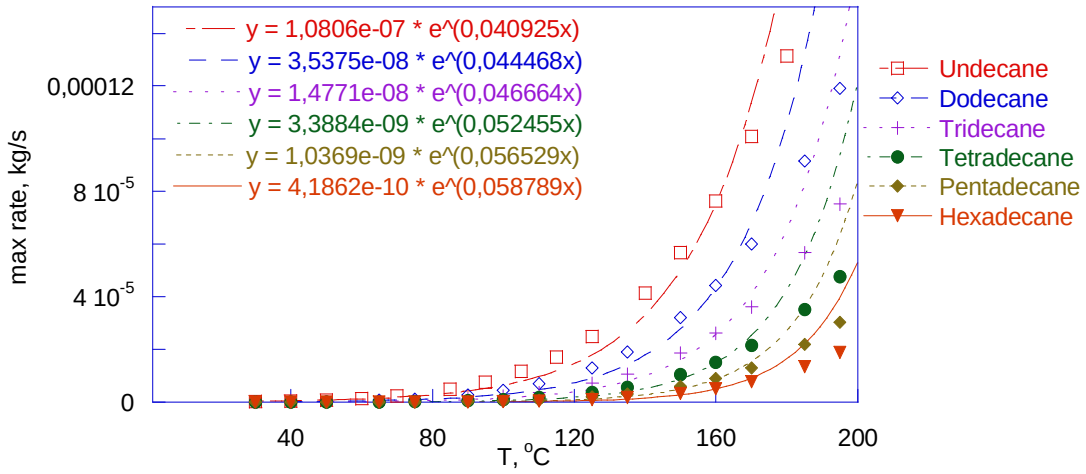

Figure 28. Theoretical maximum evaporation rates for all alkanes.

The previous analysis provides a means of understanding how the rate of evaporation changes with temperature, but additional information of evaporation is needed to develop a more encompassing model. The change of the mass of the sample with respect to time, as the temperature is increased, has been found from analyzing the data collected throughout testing. The mass of the sample as a function of time was observed to take the following form:

$$m(t) = a_3t^3 + a_2t^2 + a_1t + a_0 \quad (26)$$

which is a 3rd order polynomial and the coefficients are found experimentally and vary based on the units used for the mass measurements and between alkanes. Figure 29 is a graph of the recorded mass of the alkanes against time. Fitting a 3rd order polynomial to these data provides a means of estimating the coefficients needed to understand how the mass changes with time between the alkanes under the same temperature profiles.

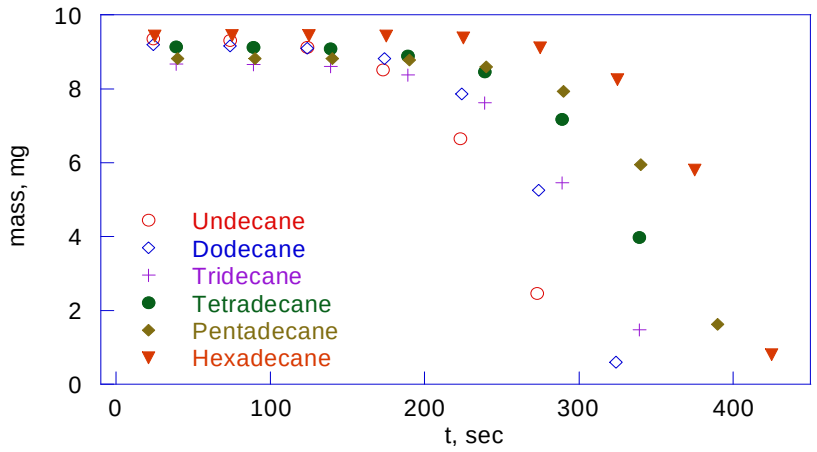

Figure 29. Mass of the alkanes versus time.

Any model that is used to predict the evaporation rate of a substance must take into account the dependency that the mass has on time as well as the dependency that the rate has on temperature. The best model for predicting evaporation rates would incorporate both of these essential characteristics.

4.3 Testing technique improvements

After conducting a series of experiments and undertaking this investigative work it has been concluded that there are some aspects of the testing techniques that can and should be improved upon in the future. As mentioned previously such factors as initial mass and initial temperature, of both the sample and equipment, are instrumental to producing consistently repeatable results. The initial mass of the samples can be monitored with the equipment used in this investigation however a greater accuracy of initial sample retrieval is needed. As discussed, the micropipettes used to retrieve the samples showed a significant variation between repeated measured sample masses. With

a more accurate micropipette, or other sampling means, would result in less iterative process for setting up tests. This is important so that the evaporation of the sample be measured at room temperature prior to an extended exposure time to ambient conditions. Another initial condition that proved to be imperative to repeatability is the initial temperature of the instrumentation. This was controlled between tests by allowing for a long resting period of the equipment to ensure a stabilization of the temperature with ambient conditions. To reduce the downtime of the equipment means of controlled cooling could be enacted. This could be done by the attaching of fins or running cooling lines to the equipment or by less invasive means such as evaporative cooling.

Replacing the equipment or constructing additional testing apparatuses could also improve the testing technique. If the testing were done inside a vacuum then the partial pressures could be measured directly and results would not rely on theoretical estimations. This could be done by having a coil of wire above a sample holder all inside a tube. Once a vacuum is created in the tube and heat is applied the resistance of the coil of wire will change as a function of the change in vapor pressure. This would be done simultaneously with a constant measuring of the mass of the sample. This apparatus determines the vapor pressure by the Langmuir method and together with measuring the mass loss would provide more accurate results of the evaporation rate of a substance. Since this apparatus requires the testing of a sample in a vacuum then the maximum possible evaporation rates would be recorded and compared between different samples. These results could then be compared to the testing results of this study to determine the environmental effects on the rate of evaporation. Additional information on this particular type of apparatus can be found in [42].

References

1. Jay Bolemon, 'Physics A Window on Our World', Prentice Hall, Englewood Cliffs, New Jersey (1995)

2. R. A. Serway, J. W. Jewett, 'Physics: for Scientists and Engineers, 6th Edition', Brooks/Cole Thomson Learning, Belmont, California (2004)

3. W. Stiver, D. Mackay, *Evaporation Rate of Spills of Hydrocarbons and Petroleum Mixtures*, Environ. Sci. Technol. Vol. 18 No. 11, pp. 834-840 (1984)

4. *Evaporation and Intermolecular Attractions*, CHM151 LL: General Chemistry I Lab Manual, pp. 115-124

5. *Science In Motion: Evaporation and Intermolecular Attractions*, Chemistry Lab 021, University of Pittsburgh at Bradford

6. C. L. Stanitski, L. P. Eubanks, C. H. Middlecamp, W. J. Stratton, 'Chemistry In Context: Applying Chemistry To Society, 3rd Edition', McGraw Hill, New York (2000)

7. A. A. Mills, J. D. Fry, *Rate of Evaporation of Hydrocarbons from a Hot Surface: Nukiyama and Leidenfrost Temperatures*, Eur. J. Phys. Vol. 3, pp. 152-154 (1982)

8. F. C. Neidhardt, J. L. Ingrahm, M. Schaechter, 'Physiology of the Bacterial Cell', Sinauer Associates Inc (1990)

9. T. A. McMeekin, J. Olley, T. Ross, D. A. Ratkowsky, 'Predictive Microbiology: Theory and Application (Innovation in Microbiology, No 5)', John Wiley & Sons (1993)

10. P. Aggarwal, D. Dollimore, K. Alexander, *The Use of Thermogravimetry to Follow the Rate of Evaporation of an Ingredient Used in Perfumes*, Journal of Thermal Analysis Vol. 49, pp. 595-599 (1997)

11. 'The Columbia Encyclopedia, Sixth Edition', Columbia University Press. (2004)

12. S. F. Mason, 'Main Currents of Scientific Thought: A History of the Sciences', Henry Schuman, New York (1953)

13. World wide web: chemistry-dictionary.com

14. V. Majer, V. Svoboda, J. Pick, 'Heats of Vaporization of Fluids', Elsevier Science Publishers (1989)

15. World wide web: nobelprize.org

16. E. Kostiner, N. D. Jespersen, 'Chemistry, 2nd Edition', Barron's Educational Series (2003)

17. T. Boublík, V. Fried, E. Hála, 'The Vapour Pressure of Pure Substances', Elsevier Scientific Publishing Co. (1973)

18. D. G. Miller, Ind. Eng. Chem. Vol. 56 Issue 3, pp. 46 (1964)

19. C. R. Antoine C., Acad. Sci., Paris, pp. 107, 681, 836, 1143 (1888)

20. C. B. Willingham, W. J. Taylor, J. M. Pignocco, F. D. Rossini, J. Res. Natl. Bur. Stand. Vol. 35, pp. 219 (1945)

21. C. L. Yaws, 'Yaw's Handbook of Thermodynamic and Physical Properties of Chemical Compounds', Golf Publishing Co. (2007)

22. R. M. Stephenson, S. Malanowski, 'Handbook of the Thermodynamics of Organic Compounds', Elsevier Scientific Publishing Co. (1987)

23. N. A. Lange, 'Lange's Handbook of Chemistry', McGraw Hill (1985)

24. D. R. Bloch, 'Organic Chemistry Demystified', McGraw Hill "Demystified" Series (2006)

25. D. Dollimore, T. A. Evans, Y. F. Lee, F. W. Wilburn, Thermochim. Acta, Vol. 198 Issue 249 (1992)

26. E. Hahne, U. Grigull, 'Heat Transfer in Boiling', Hemisphere Publishing Co. (1977)

27. H. N. V. Temperley, 'Changes of State', Cleaver-Hume Press Ltd. (1956)

28. S. F. Wright, P. Phang, D. Dollimore, K. S. Alexander, *An Overview of Calibration Materials Used in Thermal Analysis—Benzoic Acid*, Thermochimica Acta, Vol. 392-393, pp. 251-257 (2002)

29. Y. Cheng, Y. Huang, K. Alexander, D. Dollimore, *A Thermal Analysis Study of Methyl Salicylate*, Thermochimica Acta, Vol. 367-368, pp. 23-28 (2001)

30. S. F. Wright, K. A. Alexander, D. Dollimore, *The Initial Thermal Characterization of Hair Color Rinse Ingredients – Adipic Acid*, Thermochimica Acta, Vol. 367-368, pp. 29-35 (2001)

31. L. Shen, K. S. Alexander, D. Dollimore, *A Thermal Analysis Study of Myristic Acid*, Thermochimica Acta, Vol. 367-368, pp. 69-74 (2001)

32. World wide web: tains.com

33. R. T. Smith, R. B. Minton, 'Calculus, 2nd Edition', McGraw Hill (2002)

34. R. Tuckermann, S. Bauerecker, B. Neidhart, *Evaporation Rates of Alkanes and Alkanols from Acoustically Levitated Drops*, Anal Bioanal Chem Vol. 372, pp. 122-127 (2002)

35. G. Guéna, C. Poulard, A. M. Cazabat, *Evaporating Drops of Alkane Mixtures*, Colloids and Surfaces A: Physicochem. Eng. Aspects Vol. 298, pp. 2-11 (2007)

36. M. Cachile, O. Bénichou, A. M. Cazabat, *Evaporating Droplets of Completely Wetting Liquids*, Langmuir Vol. 18, pp. 7985-7990 (2002)

37. G. Guéna, C. Poulard, A. M. Cazabat, A. Boudaoud, M. Ben Amar, *Rescaling the Dynamics of Evaporating Drops*, Collége de France, 11 place Marcelin Berthlot, 75231 Paris Cedex 05

38. K. J. Beverley, J. H. Clint, P. D. I. Fletcher, *Evaporation Rates of Pure Liquids Measured Using a Gravimetric Technique*, Phys. Chem. Chem. Phys. Vol. 1, pp. 149-153 (1999)

39. C. Pichon, V. Risoul, G. Trouvé, W. A. Peters, P. Gilot, G. Prado, *Study of Evaporation of Organic Pollutants by Thermogravimetric Analysis: Experiments and Modeling*, Thermochimica Acta Vol. 306, pp. 142-151 (1997)

40. T. K. Xia, U. Landman, *Molecular Evaporation and Condensation of Liquid n-Alkane Films*, J. Chem. Phys. Vol. 101 Issue 3 (1994)

41. I. Langmuir, Phys. Rev. 2, 329 (1913); 8, 149 (1916); Phys. Z. 14, 1273 (1913); J. Am. Chem. Soc. 38, 2221 (1916)

42. A. N. Nesmeyanov, 'Vapor Pressure of the Chemical Elements', Elsevier Publishing Co., New York (1963)

43. J. R. Ogden, M. Fogiel, 'The Organic Chemistry Problem Solver: A Complete Solution Guide to any Textbook', Research and Education Associates, New York (1993)

44. N. A. Vasilieva, R. A. Buyanov, *Radical Generation during Pyrolysis of n-Undecane on $BaCl_2$ and Imperfect magnesium oxides*, Chemistry for Sustainable Development Vol. 12, pp. 641-647 (2004)

45. J. M. Hanback, 'Organic Chemistry', Thomson Brooks/Cole, New York (2005)

46. V.R. Dushin, A.V. Kulchitskiy, V.A. Nerchenko, V.F. Nikitin, E.S. Osadchaya, Yu.G. Phylippov, N.N. Smirnov, *Mathematical simulation for non-equilibrium droplet evaporation*, Acta Astronautica, Vol. 63 Issues 11-12, pp. 1360-1371 (2008)

47. Sandra C.K. De Schepper, Geraldine J. Heynderickx, Guy B. Marin, *Modeling the evaporation of a hydrocarbon feedstock in the convection section of a steam* cracker, Computers & Chemical Engineering, In Press, Corrected Proof, Available online 5 August 2008

48. Giorgos Mellios, Zissis Samaras, *An empirical model for estimating evaporative hydrocarbon emissions from canister-equipped vehicles*, Fuel, Vol. 86 Issue 15, pp. 2254-2261 (2007)

49. A.B. Shigarov, A.A. Bocharov, V.A. Kirillov, *Analysis of stability of the interphase front with evaporation and exothermic reaction in the porous catalyst slab*, Chemical Engineering Science, Vol. 62 Issue 17, pp. 4770-4779 (2007)

50. Jerónimo Merino, Verónica Bucalá, *Effect of temperature on the release of hexadecane from soil by thermal treatment*, Journal of Hazardous Materials, Vol. 143 Issues 1-2, pp. 455-461 (2007)

51. Hongzhe Tian, Jing Xu, Yuan Xu, Yafeng Guan, *Multidimensional liquid chromatography system with an innovative solvent evaporation interface*, Journal of Chromatography A, Vol. 1137 Issue 1, pp. 42-48 (2006)

52. Ho-Saeng Lee, Jung-In Yoon, Jae-Dol Kim, P.K. Bansal, *Characteristics of condensing and evaporating heat transfer using hydrocarbon refrigerants*, Applied Thermal Engineering, Vol. 26 Issue 10, pp. 1054-1062 (2006)

53. Ian Snape, Susan H. Ferguson, Paul McA. Harvey, Martin J. Riddle, *Investigation of evaporation and biodegradation of fuel spills in Antarctica: II—Extent of natural attenuation at Casey Station*, Chemosphere, Vol. 63 Issue 1, pp. 89-98 (2006)